

Review

Interfacial Layer Engineering for Performance Enhancement in Polymer Solar Cells

Hao Zeng, Xucheng Zhu, Yongye Liang * and Xugang Guo *

Department of Materials Science and Engineering, South University of Science and Technology of China, No. 1088, Xueyuan Rd., Guangdong, Shenzhen 518055, China;

E-Mails: zengh@mail.sustc.edu.cn (H.Z.); zhuxc@mail.sustc.edu.cn (X.Z.)

* Authors to whom correspondence should be addressed; E-Mails: liang.yy@sustc.edu.cn (Y.L.); guo.xg@sustc.edu.cn (X.G.); Tel.: +86-755-8801-8306 (Y.L.); +86-755-8801-8307 (X.G.); Fax: +86-755-8801-8904 (Y.L. & X.G.).

Academic Editor: Nanjia Zhou and Robert P.H. Chang

Received: 28 November 2014 / Accepted: 9 February 2015 / Published: 17 February 2015

Abstract: Improving power conversion efficiency and device performance stability is the most critical challenge in polymer solar cells for fulfilling their applications in industry at large scale. Various methodologies have been developed for realizing this goal, among them interfacial layer engineering has shown great success, which can optimize the electrical contacts between active layers and electrodes and lead to enhanced charge transport and collection. Interfacial layers also show profound impacts on light absorption and optical distribution of solar irradiation in the active layer and film morphology of the subsequently deposited active layer due to the accompanied surface energy change. Interfacial layer engineering enables the use of high work function metal electrodes without sacrificing device performance, which in combination with the favored kinetic barriers against water and oxygen penetration leads to polymer solar cells with enhanced performance stability. This review provides an overview of the recent progress of different types of interfacial layer materials, including polymers, small molecules, graphene oxides, fullerene derivatives, and metal oxides. Device performance enhancement of the resulting solar cells will be elucidated and the function and operation mechanism of the interfacial layers will be discussed.

Keywords: polymer solar cells; anode interfacial layers; cathode interfacial layers; polymer interfacial layers; small molecule interfacial layers; graphene oxides; fullerene derivatives; metal oxides

1. Introduction

As a new clean and sustainable energy source, organic solar cells (OSCs) have received a great amount of attention from both academia and industry in the past three decades [1–3]. In comparison with conventional inorganic semiconductors-based solar cells, OSCs offer unique advantages in terms of materials processing, device fabrication, and device functionalities [4,5]. The active layers can be deposited via solution-based techniques, such as spin-coating or printing, which enable massive device production at low temperature, and hence greatly reduce device cost [4,6]. Moreover, OSCs can be readily integrated onto flexible or rollable substrates, such as plastics and fabrics; therefore, new functionalities can be realized in OSCs, such as light weight and mechanical flexibilities [7,8].

On the basis of the chemical structures of the active layer components, specifically the electron donor (p-type) semiconductors, OSCs can be further divided into two sub-categories: *i.e.*, small molecule solar cells [9–11] and polymer solar cells (PSCs) [12–16]. Current state-of-the-art OSCs feature an interpenetrating network (bulk heterojunction) comprising of polymer semiconductors as the electron donors and fullerene derivatives as the electron acceptors [17], which was invented by Heeger [18] and Friend [19] in 1995, independently. PSCs typically exhibit improved performance in comparison to small molecule-based solar cells [9,10,13], which could be mainly attributed to the better absorption of solar irradiation enabled by the smaller band gaps of polymer semiconductors [3,12,20,21] *versus* small molecules, and more efficient exciton dissociation and charge transport and collection in the interpenetrating polymer/fullerene network *versus* small molecule/fullerene blend [22–24]. The device performance of PSCs has been greatly improved in the last couple of years and now the highest power conversion efficiencies (PCEs) of PSCs have reached 10.8% [25–28]. The performance improvement of PSCs is mainly attributed to the materials development [3,12], film morphology and microstructure optimizations [22,29], and device engineering [23,25,26].

The photovoltaic effect in laminated organic materials system was first discovered by Kearns and Calvin in 1958 [30], and the first OSC containing a single flat bilayer heterojunction was invented by Tang in 1986. In Tang's cells [31], an n-type semiconductor, perylene tetracarboxylic derivative, is stacked on top of a p-type copper phthalocyanine semiconductor. Due to the limited n-type semiconductor/p-type semiconductor interface (heterojunction) area, only excitons formed within a distance of ~20 nm from the heterojunction can reach the interface and then dissociate into free charge carriers [1]. Excitons generated away from the interfaces with a distance >20 nm generally cannot dissociate, therefore the PCEs of flat bilayer OSCs are typically small (<6%) [32,33]. The bulk heterojunction (BHJ) cells developed by Heeger [18] and Friend [19] lead to the formation of interpenetrating network with nanoscale phase separation in the active layer consisting of a polymer donor and a fullerene derivative acceptor. The BHJ solar cells show substantially improved PCEs *versus* the bilayer solar cells, which is mainly attributed to the dramatically enhanced exciton dissociations.

The excitons generated in the BHJ blend can reach the interfaces and then separate into free charge carriers, electrons and holes, when the nanoscale phase separation in BHJ film is achieved [29].

The invention of BHJ solar cells greatly improves the PCEs of PSCs, which is mainly attributed to the more efficient exciton dissociations enabled by the maximized heterojunction interface and increased charge carrier collection attributed to the formation of interpenetrating network. The BHJ solar cells provide bicontinuous pathways for the charge carriers to migrate to their respective electrodes. However, the donor semiconductor and the acceptor semiconductor are randomly distributed in the active layer, and hence both the donor semiconductor and the acceptor semiconductor could be in intimate contact with the anode and cathode in the BHJ solar cells. The charge carriers are therefore likely to recombine at electrodes, which can detrimentally lower the PCEs of PSCs. In order to mitigate the charge carrier recombination at the electrodes, various interfacial layer (IFL) materials have been developed to selectively allow the desired charge carriers to pass through and in the meantime block the undesired carriers (Figure 1); therefore, charge carrier recombination at electrodes can be substantially suppressed and the PCEs can be significantly improved for the cells with engineered IFLs [34–37]. The interfacial layers can also greatly lower the contact resistance, which is detrimental to device performance. Choosing appropriate IFL materials with optimized layer thickness can substantially enhance the device performance of PSCs. In addition to the electrical effects, the IFLs also show significant impacts on light distribution and absorption [38]. It is evident that solar cell performance is strongly dependent on the intensity of the absorbed light. It has been shown that appropriate choice of IFLs can greatly increase the light absorption by reducing the parasitic reflection of light at interfaces. At the same time, in order to maximize the PCEs, the light absorption should be maximized within the active layer. Therefore, the light absorption by any other components including IFLs must be minimized. The materials that are transparent in the visible region seem to be highly desirable for maximizing PCEs.

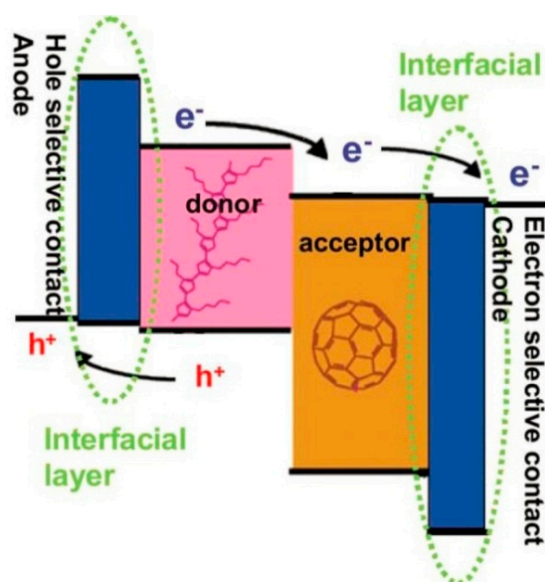


Figure 1. Schematic illustration of a polymer solar cell in extraction mode. Excitons are generated and diffuse to the donor/acceptor (bulk heterojunction) interface where the excitons dissociate to free charge carriers. The charge carriers are then transported to the electrodes and are extracted by the interfacial layers to the respective electrodes. Reprinted with permission from [36]. Copyright 2010 Royal Society of Chemistry.

Moreover, the IFLs can also act as optical spacers by modifying the optical distribution of light intensity in the active layers. TiO_x has been successfully employed as optical spacer to increase device performance of PSCs [38]. Plasmonic effect induced by the incorporation of metallic nanoparticles can greatly increase the light absorption by generating localized intensification of the electromagnetic field [39]. Therefore, IFLs with dispersed metal nanoparticles show positive effects on improving device performance of PSCs [40].

Interfacial layer engineering is accompanied by the surface energy change of IFLs, which could lead to improved interactions between active layers and IFLs and have shown profound impacts on film morphology of active layers, and thereby the device performance of PSCs [23]. The active layer with favored vertical phase degradation demonstrates improved performance than the blends without such morphology due to the suppressed charge recombination [23,41]. Furthermore, The IFLs play a critical role in terms of improving device performance stability, which is essential for the real-world applications [42]. IFL engineering can also significantly alter work function of electrodes enabled by the formation of a dipole moment, and high work function metals such as Ag and Au with better air stability then can be used as the electrodes [43]. Moreover, IFLs can effectively block the diffusion of unwanted species from electrodes, such as metal particles, during device fabrication and operation, which can prohibit the chemical and physical reactions between the active component and the electrode [44]. IFLs can absorb UV radiation from sun and provide a certain degree of protection against photo-oxidation for the active layer. Finally, hydrophobic and dense IFLs can hinder the penetration of water and oxygen and function as scavenger for these species, which increases the durability of PSCs.

Hence, IFL engineering has been one of the most active research fields in PSCs, various IFL materials with tunable properties have been developed and incorporated into PSCs in the last couple of years. Considering the significance of IFLs in improving the device performance, the advancement of PSCs is closely related to IFL engineering, and actually the most promising device performance with enhanced solar cell stability is obtained from the PSCs with engineered IFLs [25,26,45]. In this review, we mainly focus on recent progress of IFL engineering of PSCs in the last couple of years, but significant works from earlier literatures will also be reviewed. For more thorough earlier works, we would like to redirect the readers to the earlier reviews [35,36,46]. This work is mainly organized based on the materials types of the IFLs, including polymers, organic small molecules, fullerene derivatives, metal oxides, and emerging novel IFLs, such as graphene oxide and its derivatives.

2. Polymer-Based Interfacial Layers

2.1. *Poly(3,4-ethylenedioxythiophene)s and Polyaniline Derivatives*

Poly(3,4-ethylenedioxythiophene) (PEDOT, Figure 2) was developed in the late 1980s in the research laboratories of Bayer AG (Leverkusen, Germany), and it was the first IFL material used in PSCs in 1998 [47] by following its successful applications in the field of organic light-emitting diodes (OLEDs) [48], or in a more conscious way in 2002 [49]. It remains its popularity in manifold ways till now. PEDOT can smooth the underlying layers, transport holes, and block electrons by forming ohmic contact with donor semiconductors in the blend, which is attributed to its high work function of

5.0–5.1 eV. Due to the low solubility and limited processability of PEDOT in organic solvents, poly(styrenesulfonic acid) (PSS, Figure 2) is commonly used with PEDOT to form a PEDOT:PSS dispersion. The PEDOT:PSS film can be deposited from its aqueous solution, and shows its robustness in resisting organic solvents in the subsequent active layer deposition. The PEDOT:PSS has been the most widely used IFL material for PSCs, which is attributed to its appropriate work function, high conductivity, excellent stability, good transparency in the visible range, easy processability, and insolubility in common organic solvents.

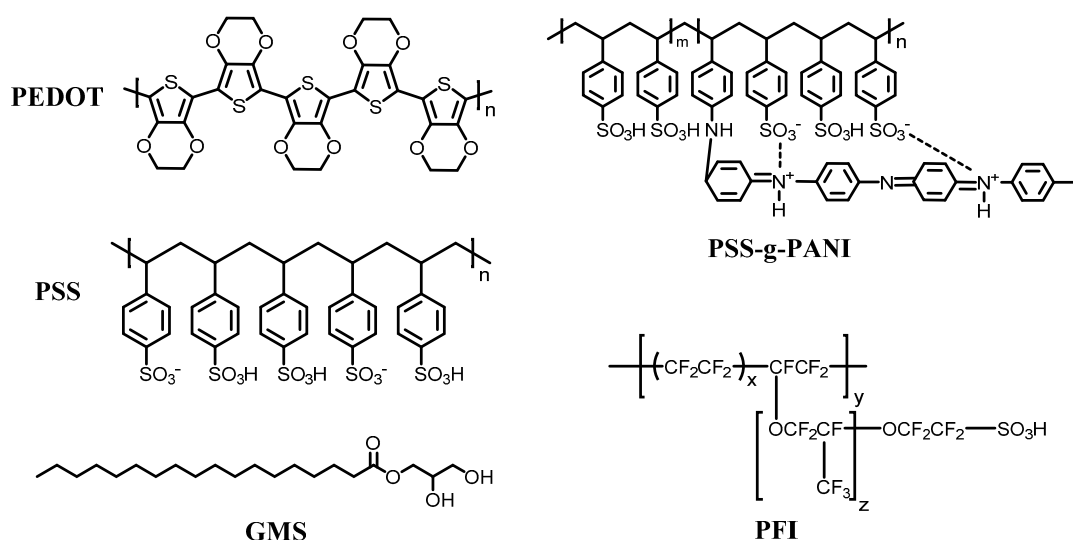


Figure 2. Chemical structure of poly(3,4-ethylenedioxythiophene) (PEDOT), poly(styrenesulfonic acid) (PSS), GMS (glycerol monostearate), poly(4-styrenesulfonate)-g-polyaniline (PSS-g-PANI), and PFI (perfluorinated ionomer) for interfacial layer materials in polymer solar cells.

Frohne and coworkers systematically modified the work function of PEDOT:PSS films electrochemically [50,51]. The treatment of electrically polymerized PEDOT film in the presence of sodium-neutralized PSS resulted in PEDOT:PSS films with work function variations up to 1.3 eV, depending on the doping level. The PEDOT:PSS film was then incorporated into poly[2-methoxy-5-(3',7'-dimethyloctyloxy)-1,4-phenylenevinylene] (MDMO-PPV)/[6,6]-phenyl-fullerene-butyric acid methyl ester (PCBM) solar cells as the hole-transporting layer, and the compensation voltage, V_0 (V_0 is the potential at which the photocurrent equals the dark current, which is proportional to the V_{oc}) tracks the work function of PEDOT:PSS. However, as the work function of PEDOT:PSS is beyond 0.3 V *versus* Ag/AgCl, the V_0 plateaus [51]. Later, Li and coworkers found that the photovoltaic performance of poly(3-hexylthiophene) (P3HT):PCBM solar cells can be improved by incorporating a PEDOT:PSS IFL between the indium tin oxide (ITO) and the active layer [52]. Kim *et al.*, carried out the studies of the effect of the thickness and the thermal annealing of PEDOT:PSS (Figure 2, Baytron P standard grade, HC Starck, Leverkusen, Germany) anode IFL on the device performance of P3HT:[6,6]-phenyl- C_{61} -butyric acid methyl ester (PC_{61}BM) bulk heterojunction PSCs [53]. It was found that the solar cell performance is greatly improved by inserting a PEDOT:PSS layer, but the PCE is not highly sensitive to the IFL thickness. Without using PEDOT:PSS, the PSCs show a sigmoidal $J-V$ shape (Figure 3), which is attributed to the barrier between ITO and active layer. After incorporation of the PEDOT:PSS

layer, the PSCs achieve substantially increased short-circuit current densities (J_{sc}) and fill factors (FF s), which is attributed to the enhanced efficiency of hole transfer between donor polymer P3HT and contact for hole transfer. The insertion of PEDOT:PSS also leads to enlarged open-circuit voltage (V_{oc}). As a result, the PSCs with PEDOT:PSS IFL showed an improved PCE by a factor of 1.8 *versus* the cells without such layer. As PEDOT:PSS thickness increased, the J_{sc} decreased, but the overall efficiency was not highly sensitive to the IFL layer thickness over a wide range of 60–165 nm. The effect of thermal annealing of PEDOT:PSS IFL (~ 70 nm) was carried out, and it was found that thermal annealing at high temperature (200–230 °C) led to slightly increased J_{sc} but decreased FF , which was attributed to the variation in conductivity and surface roughness of PEDOT:PSS layers with annealing temperature. The V_{oc} showed small changes during thermal annealing, which was attributed to the good ohmic contact between PEDOT:PSS IFL with P3HT.

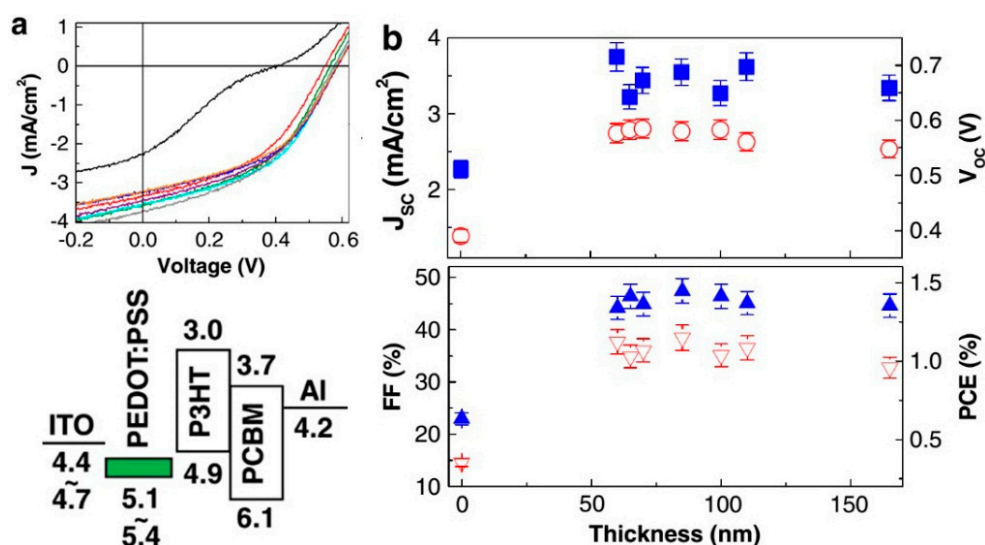


Figure 3. (a) (up) $J-V$ characteristics (AM 1.5, 85 mW/cm²) of polymer solar cells with non-annealed P3HT:PCBM layer (70 nm) and non-annealed PEDOT:PSS layer of which thickness is 0 (ITO only; black line), 60 (gray line), 65 (orange line), 70 (purple line), 85 (sky blue line), 100 (blue line), 110 (green line), and 165 nm (red line). (Down) Ideal flat energy band diagram for the device with the PEDOT:PSS IFL layer; (b) J_{sc} (filled squares), V_{oc} (open circles), FF (filled upward triangles), and PCE (open downward triangles) as a function of PEDOT:PSS IFL thickness. Reprinted with permission from [53]. Copyright 2009 Elsevier B.V.

The PEDOT:PSS IFL has showed great success in improving the device performance of PSCs in the last decade, but it has several implications due to its high acidity (pH: $\sim 1-3$) and its hydrophilic character. The acidic character can lead to ITO deterioration and the hydrophilic nature can result in uptake of humidity from ambient, which causes the performance degradation when the cells are stored in air. In order to address these drawbacks, two types of approaches have been carried out: those involving physical treatment and those involving chemical additives.

The etching of ITO by acidic PEDOT:PSS and the following diffusion of indium into active layer lead to a fast deterioration of PSC performance [54,55]. Kim and coworkers studied influence of PEDOT:PSS IFL with controlled acidity on the device performance and lifetime of P3HT:PC₆₁BM

PSCs [55]. The addition of small amount of NaOH (0.2 molar ratio) can remove 23% of sulfonic acid group, but showed no degradation on PSC performance. Device stability test revealed that NaOH modified PSCs showed improved device lifetime *versus* the cells using the acidic PEDOT:PSS IFL. Wang *et al.*, reported the replacement of acidic PEDOT:PSS (AI 4083, pH = 1–3; H.C. Starck GmbH, Goslar, Germany) with pH-neutral PEDOT:PSS (Jet N; H.C. Starck GmbH) as the anode IFL for PSCs [56]. The incorporation of pH-neutral PEDOT:PSS and the treatment of the neutral PEDOT:PSS with UV-ozone and oxygen plasma led to the ITO/PEDOT:PSS/poly[*N*-9'-heptadecanyl-2,7-carbazole-*alt*-5,5-(4,7-di-2-thienyl-2',1',3'-benzothiadiazole)] (PCDTBT):[6,6]-phenyl-C₇₁-butyric acid methyl ester (PC₇₁M)/Al solar cells with an enhanced PCE of 6.60%. The cells using acidic PEDOT:PSS showed a PCE of 6.28%. Scanning Kelvin probe measurement revealed that the UV-ozone treatment increases PEDOT:PSS work function from 4.75 to 4.90 V. After oxygen plasma treatment, the work function increases to 5.03 V, and the work function finally reaches 5.08 V after both UV-ozone and oxygen plasma treatment. Hence, the performance improvement is attributed to the reduction of energy offset between the hole transport IFL and the active layer after UV-ozone and oxygen plasma treatment, which increases V_{oc} , improves charge carrier transport, and prevents charge carrier recombination. The incorporation of neutral PEDOT:PSS also affords PSCs with greatly improved device stability (Figure 4). The PCEs of the cells containing acidic PEDOT:PSS decrease by 45% after 50 days' storage under ambient conditions, while the PCEs of the cells incorporating pH-neutral PEDOT:PSS decrease only by 20% after the same period under the same condition. The increased stability of the cells using pH-neutral PEDOT:PSS IFL is attributed to the reduced etching of indium from ITO and the hindered diffusion of indium into active layer [56].

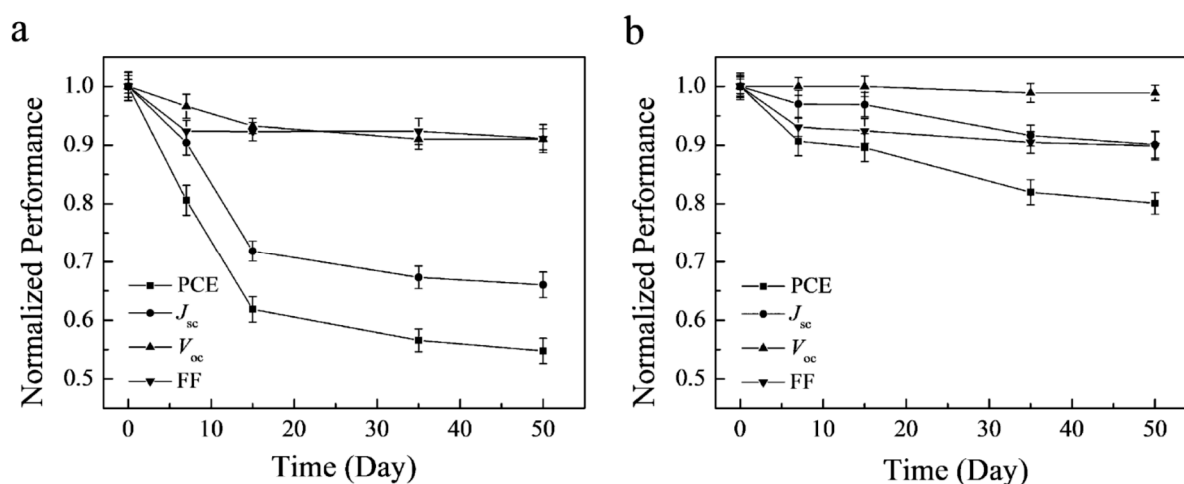


Figure 4. Dependence of the normalized device performance characteristics on storage time. (a) AI 4083 PEDOT:PSS device; and (b) UV-ozone and oxygen plasma treated Jet N PEDOT:PSS device. Reprinted with permission from [56]. Copyright 2014 American Chemical Society.

By spin-coating a surfactant layer, glycerol monostearate (GMS, Figure 2), onto the top of PEDOT:PSS (Clevios P and Clevios PH 1000; Heraeus Ltd., Hanau, Germany) film, Yang *et al.*, developed ITO-free PSCs containing a PEDOT:PSS/surfactant bilayer film as the transparent anode, therefore, the bilayer film functions not only as anode IFL, but also as electrode [57]. After GMS

modification, the PEDOT:PSS conductivity was significantly improved from ~ 1 S/cm to more than 1000 S/cm with a sheet resistance of 98 Ω /sq. The conductivity improvement is attributed to the GMS-induced segregation of PSS chains and the conformational change of the conductive PEDOT chains within PEDOT:PSS blend. The film shows a transparency of $\sim 80\%$ in visible range, which is comparable to that of widely used ITO. The conventional PSCs having the structure of PEDOT:PSS/GMS/polymer:PC₇₁BM/poly[(9,9-bis(3'-(*N,N*-dimethylamino)propyl)-2,7-fluorene)-*alt*-2,7-(9,9-dioctylfluorene) (PFN)/Al exhibit PCEs of 5.90% and 7.06% for PCDTBT and poly({4,8-bis[(2-ethylhexyl)oxy]benzo[1,2-*b*:4,5-*b'*]dithiophene-2,6-diyl} {3-fluoro-2-[(2-ethylhexyl)carbonyl]thieno[3,4-*b*]thiophenediyl}) (PTB7) cells, respectively. The 7.06% PCE is comparable to that of the traditional ITO-containing solar cells and was the highest one for ITO-free BHJ PSCs at that time. Chu and coworkers reported highly conductive PEDOT:PSS film by treating with formic acid for ITO-free PSCs [58]. The formic acid treatment can lead to four orders of magnitude increased conductivity. The highest conductivity of 2050 S/cm was obtained using 26 M formic acid. The conductivity increase is attributed to the phase separation between PEDOT and PSS, increased carrier concentration, removal of PSS, and morphology and conformation change with elongated and better connected PEDOT chain. The P3HT:PCBM solar cells using standalone PEDOT:PSS anodes treated with formic acid show a PCE of 4.10%, which is comparable to that (4.11%) of the solar cells containing the traditional ITO.

In addition to PEDOT:PSS, other conducting polymers have also been developed as hole extraction/electron blocking layers (or anode interfacial layers) for PSCs. Lee *et al.*, developed water soluble self-doped conducting polyaniline graft copolymer composites based on poly(4-styrenesulfonate)-*g*-polyaniline (PSS-*g*-PANI, Figure 2) having tunable work functions (WFs) for PSCs [59]. The value of WF was affected by the compositions of solutions, and a very high WF value (up to 6.09 eV) was obtained by simple spin-coating of blends with perfluorinated ionomer (PFI, Figure 2) even though very little PFI was added to the compositions, which was much higher than that (WF = 5.1 eV) of conventional PEDOT:PSS. XPS (X-ray photoelectron spectroscopy) characterization indicates that the PFI self-organizes at the film surface, and the high PFI concentration at surface causes a substantial WF increase due to the higher ionization potential induced by the perfluorinated chains than the common hydrocarbon chains [60]. PSCs having the structure of ITO/PSS-*g*-PANI:PFI/P3HT:PCBM/BaF₂/Al were fabricated and showed a PCE of 3.4%, which was slightly higher than that (3.2%) of ITO/PEDOT:PSS/P3HT:PCBM/BaF₂/Al cells and that (3.3%) of ITO/PSS-*g*-PANI/P3HT:PCBM/BaF₂/Al cells. The enhanced performance is attributed to P3HT enrichment on anode IFLs enabled by its low surface energy due to the PFI-enriched IFL surface and good ohmic contact between the donor semiconductor P3HT and the IFL in PSS-*g*-PANI:PFI cells. The results indicate that the water-soluble PSS-*g*-PANI composites with self-organized surface layer should be good candidates for reliable anode IFLs in PSCs.

2.2. Water/Alcohol Soluble Conjugated Polymers

Water/alcohol soluble conjugated polymers (WSCPs) are another class of polymer-based IFLs and have shown great success in facilitating charge injection in polymer light emitting diodes (PLEDs) [61]. WSCPs have been widely employed to realize high-efficiency, air-stable PLEDs. The success of WSCPs in PLEDs indicates their potential as IFL materials for PSCs [62]. In general, WSCPs are

structurally composed of two key components: π -conjugated backbone and surfactant-like solubilizing side chain, such as amino, phosphate, carboxyl, and quaternary ammonium, sulfonic and zwitterionic group. Their unique properties offer WSCPs a series of advantages: (a) the excellent solubility in highly polar solvents enables multilayer film deposition via simple solution-based processing without damaging the underlying layer using orthogonal solvents; (b) the highly polar side groups have been found to show great modifications to interfacial layer functions, hence improving device performance of PSCs; (c) the optical properties and charge transport characteristics can be manipulated via structural modifications of polymer structures. The unique properties of WSCPs have enabled the resulting PSCs to achieve state-of-the-art performance in organic solar cells [26,63].

Cao *et al.*, firstly demonstrated performance enhancement of PSCs by incorporating a water/alcohol soluble conjugated polymers as IFLs [64]. It was found that V_{oc} of poly[2,7-(9,9-dioctylfluorene)-*co*-(4,7-dithien-2-yl)-2,1,3-benzothiadiazole] (PFO-DBT35):PCBM solar cells can be greatly enhanced by 0.3 V via inserting a thin layer of poly[(9,9-bis{3'-[(*N,N*-dimethyl)-*N*-ethylammonium]propyl}-2,7-fluorene)-2,7-(9,9-dioctylfluorene)-*co*-(4,7-dithien-2-yl)-2,1,3-benzothiadiazole] (PFNBr-DBT15, Figure 5) or poly[(9,9-bis{3'-[(*N,N*-dimethyl)-*N*-ethylammonium] propyl}-2,7-fluorene)-*alt*-1,4-phenylene]dibromide (PFPNBr, Figure 5) between active layer and cathode metal electrode [64]. The PSCs using polymer IFLs show a V_{oc} of 0.95 ± 0.05 V, while the cells using routine LiF/Al and Ba/Al electrodes only demonstrate a moderate V_{oc} 0.65 ± 0.05 V. The V_{oc} enhancement can be attributed to the superposition of the built-in field with the dipole of polymer IFLs. The substantial V_{oc} increase in combination with the simplicity renders the incorporation of WSCP as an effective strategy for enhancing solar cell performance. Similarly, Xie [65] and Kim [66] reported the applications of other fluorene-based conjugated poly(9,9-bis(6'-diethoxyphosphorylhexyl)fluorene) (PF-EP, Figure 5) and a polyfluorene derivative which has hybrid quaternary ammonium end-capped alkyl/alkoxyl side chains poly[(9,9-bis((6'-(*N,N,N*-trimethylammonium)hexyl)-2,7-fluorene)-*alt*-(9,9-bis(2-(2-ethoxyethoxy)ethyl)-9-fluorene))] dibromide (WPF-oxy-F, Figure 5) for PSCs, respectively. Xie [65] found that the incorporation of 5 nm PF-EP can lead to improved V_{oc} and fill factor, and hence result in an increased PCE of 3.38% *versus* that (1.98%) of control cell. The performance enhancement was attributed to more effective prevention of hot metal atom penetration into active layer, which could result in significant electrical leakage and quenching site for excitons. Kim [66] found that the incorporation of a thin layer of WPF-oxy-F leads to a PCE of 3.77% for the P3HT:PCBM PSC, which is significantly higher than that of the control cells. The performance enhancement was attributed to the reduction of work function of Al cathode, which results in improved V_{oc} and *FF*. Cao *et al.*, further applied five distinct WSCPs as cathode interlayers for PSCs. The WSCPs include poly[(9,9-bis(3'-(*N,N*-dimethylamino)propyl)-2,7-fluorene)-*alt*-2,7-(9,9-dioctylfluorene)] (PFN, Figure 5) and its cationic conjugated polymer electrolytes (PF-X, Figure 5). The resulting WSCP-based PSCs containing polyfluorene copolymer PFO-DBT35 as the donor polymer showed increased open-circuit voltages (V_{ocs}), while for the solar cells containing P3HT and poly[2-methoxy-5-(2'-ethylhexyloxy)-*p*-phenylene vinylene] (MEH-PPV) as the donor polymers, no significant V_{oc} enhancement was observed [67]. Furthermore, it was found that the V_{oc} increase for the PFO-DBT35 based PSCs was not sensitive to the IFL materials. The origin of the V_{oc} enhancement was investigated by examining the dark currents. It was found that the dark currents were significantly suppressed when the WSCPs were used as IFLs in the PFO-DBT35 cells, which implies an increased V_{oc} according to the Shockley equation. Bazan

and coworkers demonstrated that insertion of an ultra-thin conjugated polyelectrolyte cathode IFL can be an effective strategy for increasing PCEs of PSCs [68]. The high-performance carbazole-based polymer PCDTBT was chosen as the electron donor semiconductor and two cationic poly(thiophene) derivatives, homopolymer poly[3-(6-trimethylammoniumhexyl)thiophene] (P3TMAHT) and copolymer poly(9,9-bis(2-ethylhexyl)-fluorene)-*b*-poly[3-(6-trimethylammonium-hexyl)thiophene] (PF2/6-*b*-P3TMAHT) were chosen as the cathode IFLs (Figure 6). It is interesting to note that these polythiophene derivatives function as electron transporting layer rather than hole transporting layer in PSCs, which is dramatically different from typical neutral polythiophenes with isoelectronic backbones. Therefore, the ionic side chains can significantly alter polymer backbone charge transport property. The IFLs were deposited by simply spin-coating their methanol solutions having a concentration of 0.01% (w/v) (P3TMAHT) and 0.2% (w/v) PF2/6-*b*-P3TMAHT onto the active layer. The low concentrations were used for minimizing IFL thickness and preventing possible complications due to ion motion and concomitant redistribution of internal electric fields in the device [69]. The incorporation of these novel polyelectrolyte based cathode IFLs resulted in greatly improved PCEs of 6.1% for the P3TMAHT cells and 6.2% for the PF2/6-*b*-P3TMAHT cells *versus* the PCE of 5.0% for the control devices without the polymer IFL. The $J-V$ characteristics of the device under dark condition showed that the dark current densities with the conjugate polyelectrolyte PSCs were significantly suppressed, which was consistent with the reduced leakage current and increased shunt resistance (R_{sh}). For $V > 0.8$ V, the series resistance (R_s) of control cells was greater than that of cells containing polyelectrolyte IFLs. Therefore, the performance improvement was attributed to the high R_{sh} and small R_s in the polyelectrolyte-based solar cells. However, the effect of methanol treatment on the active layer should not be excluded [68,70], and the deposition and removal of methanol on the PCDTBT:PC₇₁BM blend also led to a slight PCE increase from 5.0% to 5.3%. The performance of the solar cells using these polyelectrolyte cathode IFLs is comparable to that of solar cells using TiO_x IFLs [38], however, the deposition of polyelectrolytes is much simpler without using thermal annealing, which should benefit device fabrications.

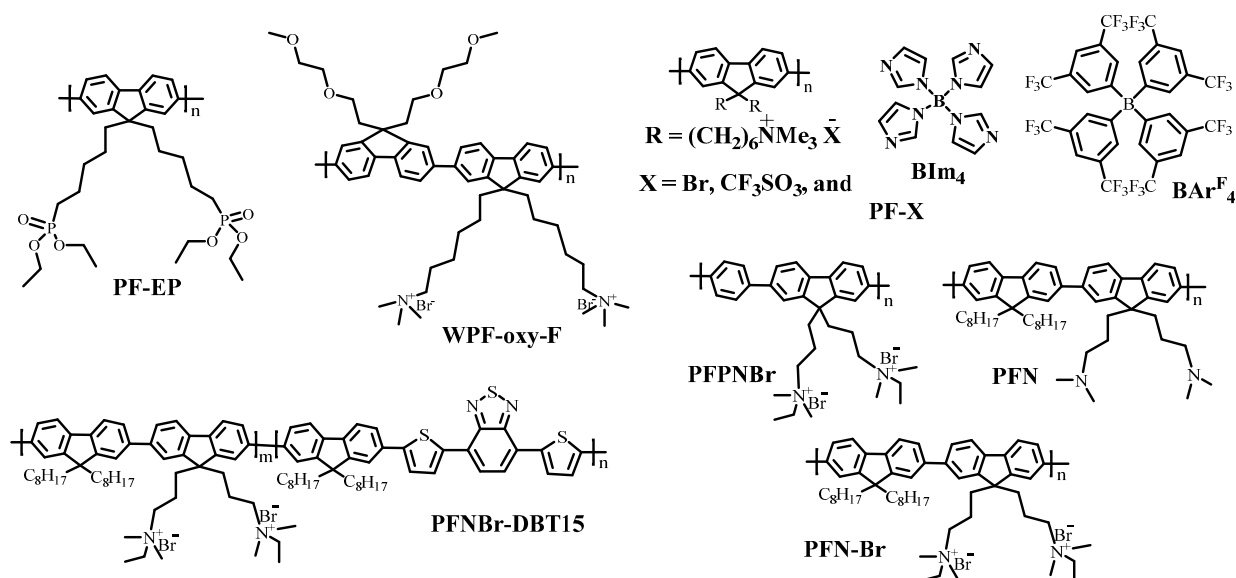


Figure 5. Chemical structures of water/alcohol soluble conjugated polymers as interfacial layer materials for polymer solar cells.

Wu and coworkers reported a simultaneous enhancement in V_{oc} , J_{sc} , and FF in PSCs containing a high-performance polymer PTB7 or PCDTBT as the electron donor and the fullerene derivative PC₇₁BM as the electron acceptor. The PSCs incorporate an alcohol/water-soluble conjugated polymer, poly[(9,9-bis(3'-(*N,N*-dimethylamino)propyl)-2,7-fluorene)-*alt*-2,7-(9,9-dioctylfluorene)] (PFN, Figure 5) as a novel cathode IFL [63]. The simultaneous enhancement in V_{oc} , J_{sc} , and FF leads to a PCE of 6.79% and 8.37% for PCDTBT and PTB7 solar cells having a structure of ITO/PEDOT:PSS/polymer:PC₇₁BM/PFN/Al, respectively. For the PCDTBT cells containing 5 nm PFN, the V_{oc} is 0.91 ± 0.02 V, which is substantially higher than that (0.71 ± 0.02 V) of the control cells without PFN cathode IFL. The effects of PFN on device performance improvement are decoded to be threefold: (a) the dipole of the interfacial layer, which leads to an enhanced built-in potential across the device; (b) the improved charge transport properties; and (c) the elimination of the buildup of the space charge and hence the reduced recombination loss due to the increase in the built-in field and charge carrier mobility.

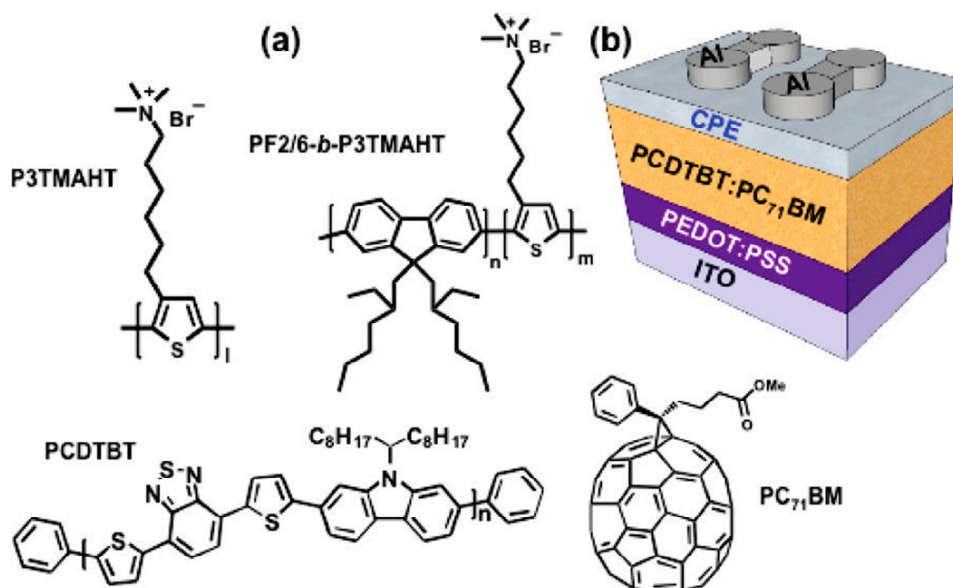


Figure 6. (a) Chemical structures of the materials used for polymer solar cells; (b) device configuration for the cells used in the study. In PF2/6-*b*-P3TMAHT, the average values of n and m were 16 and 27, respectively. Reprinted with permission from [68]. Copyright 2011 American Chemical Society.

A PFN derivative PFN-Br (Figure 5) was synthesized and employed as cathode IFL in combination with ZnO for PSCs. The cathode ZnO/PFN-Br IFL was deposited by spin-coating a ~ 40 nm thick ZnO followed by the deposition of 5 nm thick PFN-Br from its water/alcohol (1:1) solution. The formation of PFN-Br on top of the ZnO led to the decrease of ZnO work function by ~ 0.4 V [71]. Inverted PSCs were fabricated containing naphtho[1,2-*c*:5,6-*c'*]bis[1,2,5]thiadiazole and benzodithiophene-based copolymer (PBDT-DTNT):PC₇₁BM as the active layer. The cells with a structure of ITO/ZnO/PFN-Br/PBDT-DTNT:PC₇₁BM/MoO₃/Ag showed a PCE of 8.4% with a J_{sc} of 17.4 mA/cm², a V_{oc} of 0.75 V, and a FF of 61%. For the cells without PFN-Br, the inverted PSCs having a device structure of ITO/ZnO/PBDT-DTNT:PC₇₁BM/MoO₃/Ag afforded a PCE of 6.1% with a J_{sc} of 15.2 mA/cm², a V_{oc} of 0.69 V, and a FF of 55%. The enlarged V_{oc} is attributed to the different band alignments in the inverted cells with and without the PFN-Br IFL, and the increased J_{sc} is attributed to the suppressed

bimolecular recombination, the better IFL electronic conductivity, and enhanced contact between the IFL and BHJ blend film in the PFN-Br containing inverted PSCs.

By using an inverted structure, the same group demonstrated a certified PCE of 9.2% for the cells with a device structure of ITO/PFN/PTB7:PC₇₁BM/MoO₃/Al (Figure 7) [26]. The polyelectrolyte PFN was used as cathode IFL, which is different from many other inverted PSCs reported in the literature, where n-type metal oxides are typically used. The deposition of thin PFN layer can greatly reduce the work function of ITO from 4.7 to 4.1 eV (Figure 7) as revealed by the X-ray photoelectron spectroscopy (XPS) measurement. As a result, the PFN modified ITO electrode can form ohmic contact with PC₇₁BM in the active layer to facilitate charge carrier collections. The inverted PSCs also enable stronger photon harvest from the solar irradiation verified by reflectance spectra measurements on real devices. The inverted PSC show decreased reflectance over a wide range of spectra (400–800 nm) *versus* that of the conventional PSCs, which leads to a remarkable improved J_{sc} of $\sim 17.5 \text{ mA cm}^{-2}$ in comparison to the J_{sc} of 15.4 mA cm^{-2} in conventional cells. The inverted PSCs also afford enhanced device stability, which should be beneficial for the real-world applications.

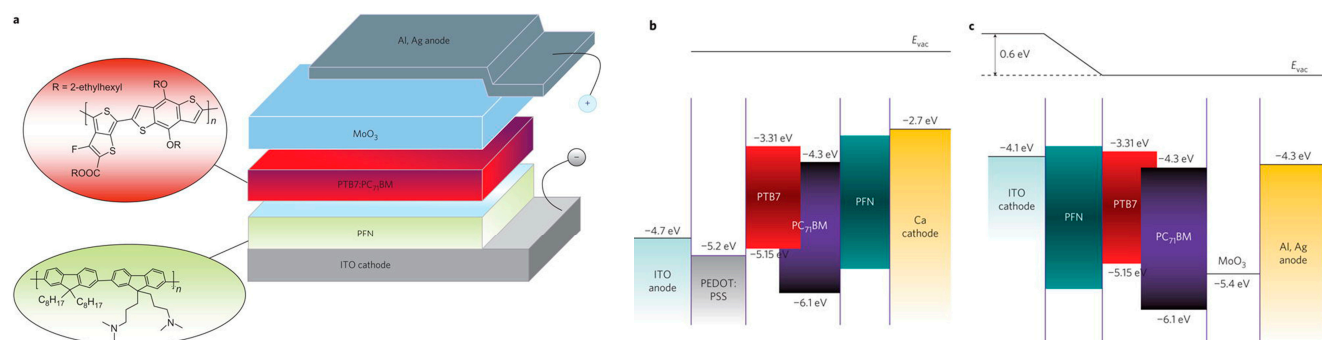


Figure 7. Schematic illustration of the inverted PTB7:PC₇₁BM PSCs, in which the photoactive layer is sandwiched between a PFN-modified ITO cathode and an Al, Ag-based top anode (a). Schematic energy levels of the conventional (b) and inverted (c) devices under flat band conditions. Note that the formation of a positive interface dipole moment (taking the dipole moment directed outwards to be positive) is presented in the inverted cells. Reprinted with permission from [26]. Copyright 2012 Nature Publishing Group.

Kippelen and coworkers reported the use of an ultrathin (1–10 nm) layer of insulating polymers containing simple aliphatic amine groups (Figure 8) as anode IFL as a “universal” approach to reducing the work function of various conductors [43]. The polymers, polyethylenimine ethoxylated (PEIE) and branched polyethylenimine (PEI), can be readily processed in air using environmentally friendly solvents such as water and methoxyethanol, and can be easily physisorbed onto the electrode surface. Due to their wide band gaps ($\sim 6 \text{ eV}$), PEIE and PEI should function as surface modifier rather than charge injection/collection layer. Charge carriers are injected via tunneling or thermionic injection processes. The work function of electrodes can be reduced over a wide range. Ultraviolet photoemission spectroscopy (UPS) measurements show substantial work function (WF) reduction after deposition of an ultrathin PEIE layer (Figure 8), the WF is reduced from 4.95 to 3.32 eV for PEDOT:PSS, from 4.40 to 3.30 eV for ITO, and from 4.70 to 3.40 eV for Au. The substantial WF reduction is induced by the intrinsic dipole moment of the neutral amine group and the charge transfer character between

interfacial layer and electrode surface. PSCs with a structure of ITO/PEIE/P3HT:1',1'',4',4''-tetrahydro-di[1,4]methanonaphthaleno[1,2:2',3',5,6:2'',3'''] [5,6]fullerene-C60 (ICBA)/MoO₃/Ag show a PCE of 5.9%, which is comparable to the device performance previously reported from their inverted cells using the same active layer [72]. The PEIE-based PSCs using another active layer of poly[(4,8-bis-(2-ethylhexyloxy)-benzo[1,2-b;4,5-b']dithiophene)-2,6-diyl-alt-(4-(2-ethylhexanoyl)-thieno [3,4-b]thiophene))-2,6-diyl] (PBDDTTT-C):PC₆₀BM exhibit a PCE of 6.6%, which is larger than that (6%) of the cells having the structure of ITO/PEDOT:PSS/PBDDTTT-C:PC₆₀BM/Ca/Al. When using PEIE modified Ag as the cathode and MoO₃ modified Ag as the anode, the PSCs have the same metal as both anode and the cathode, the resulting PSCs having the structure of ITO/Ag/PEIE/P3HT:ICBM/MoO₃/Ag show a PCE of 2.6%. The performance is mainly limited by the low transmittance of Ag electrode.

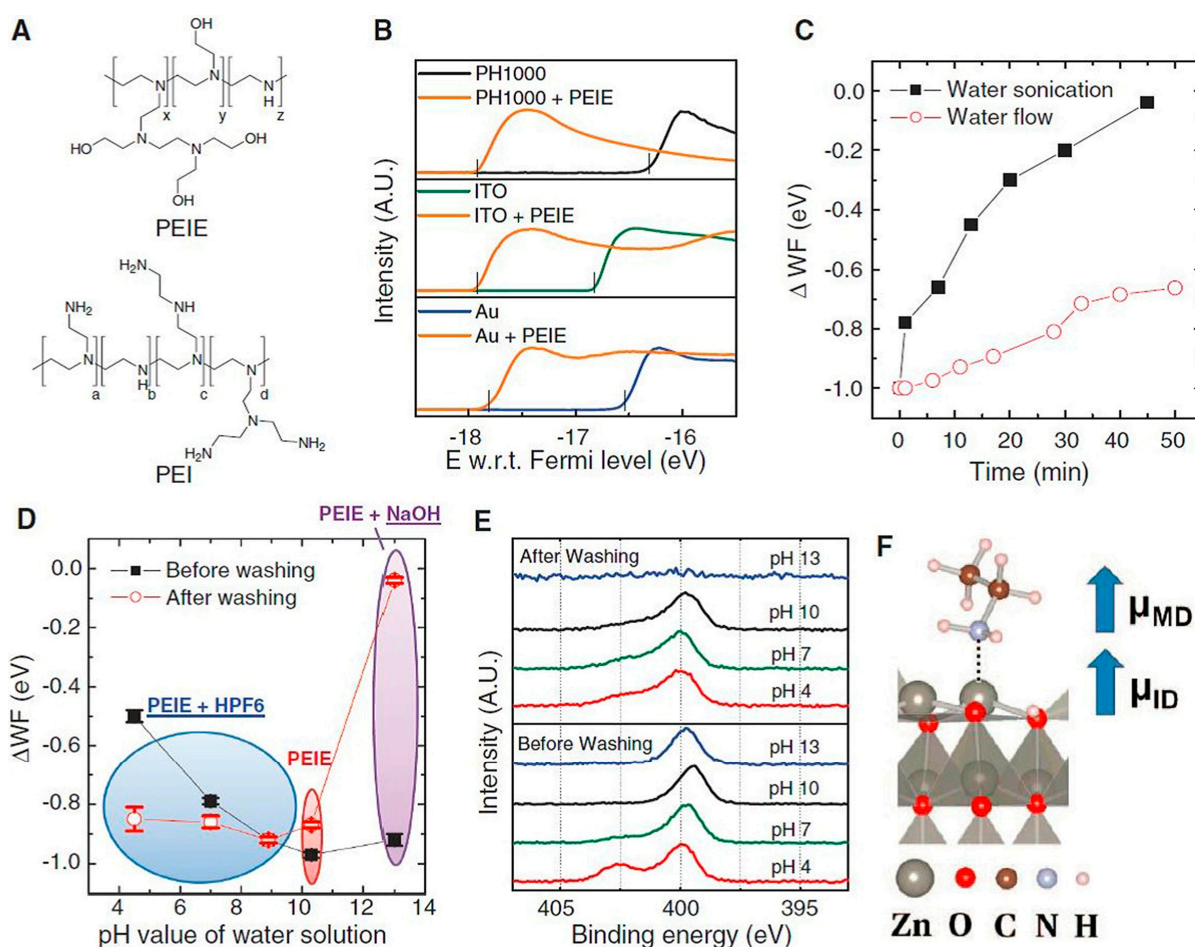


Figure 8. (A) Chemical structure of polymer IFL materials PEIE and PEI; (B) Photoemission cutoff obtained via UPS for high conductivity PEDOT:PSS PH1000 (H.C. Starck Inc., Newton, MA USA), ITO, and Au samples, with and without PEIE; (C) WF variation, relative to bare ITO, of ITO/PEIE after different washing conditions; (D) WF variation, relative to bare ITO, upon modification from PEIE water solution, PEIE with hexafluorophosphoric acid (HPF₆) water solution, and PEIE with NaOH water solution before (solid squares) and after (open circles) water washing; (E) N1s core level recorded via XPS on the samples in (D) before and after washing; (F) Proposed model of molecular dipole-induced and surface dipole-induced WF reduction on ZnO surface. Reprinted with permission from [43]. Copyright 2012 American Association for the Advancement of Science.

Recently, Kim and coworkers reported electron-rich PEI as cathode modifier layer, which was in combination with electron-collecting ZnO to form a bilayer cathode IFL for PSCs [73]. The PEI thickness need be minimized to 2 nm due to its insulating character. The conduction band of ZnO is lowered enabled by the dipole moment formation between ZnO film and PEI monolayer, which results in enhanced PCEs. Moreover, the PEI monolayer can improve the surface roughness of ZnO, which decreases device series resistance. The corresponding PSCs having the device structure of ITO/ZnO/PEI/PTB7:PC₇₁BM/MoO₃/Ag show a PCE up to 8.9%, which is comparable to the best PCE reported using conjugated polymer electrolyte IFLs [26,67]. While the cells containing only ZnO or PEI cathode IFL show decreased PCEs of 6.99% and 7.49%, respectively. The performance enhancement is mainly enabled by the increased J_{sc} and FF in ZnO/PEI cells, which is attributed to the fast electron transport. The PEI deposition leads to improved physical contact between the ZnO/PEI layer and the BHJ film due to the smoother surface (1.89 nm) of the PEI-coated ZnO layer compared to that (2.23 nm) of ZnO layer without the PEI monolayer. Moreover, PEI shows good compatibility with other metal oxides to form bilayer hybrid cathode IFLs. Recently, Li *et al.*, reported TiO_x/PEI film as the electron transporting layer for high-performance PSCs, the resulting PTB7:PC₇₁BM inverted cells achieve an average PCE of 8.72% with a champion value of 9.08%, which is much greater than that (7.38%) from the control cells using TiO_x IFL [74].

3. Small Molecules

In addition to polymers, organic small molecules are also highly promising IFL materials for performance enhancement and stability improvement in PSCs. In comparison to polymer IFLs, small molecule-based ones could achieve some attractions, such as easy purification, monodispersity, and well-defined structure, and better batch-to-batch reproducibility, which should benefit PSC applications. Hence, various small molecule IFL materials are designed, synthesized, and implemented in PSCs with excellent performance.

Inspired by the success for reducing electron injection barrier in organic light emitting diodes (OLEDs), commercial available pigment quinacridone derivatives sodium N,N'-bis(6-sulfonylhexyl)quinacridone (Na⁺QHSO₃⁻, Figure 9) was employed as cathode IFL in PSCs, which led to an improved FF and hence an improved PCE [75]. Na⁺QHSO₃⁻ shows good solubility in polar solvent and can be deposited from its methanol solution. The PSC with the structure of ITO/PEDOT:PSS/PCDTBT (or poly[2,6-(4,4-bis-(2-ethylhexyl)dithieno[3,2-*b*:2',3'-*d*]silole)-*alt*-4,7-(2,1,3-benzothiadiazole)] (Si-PCPDTBT)): PC₇₁BM/Na⁺QHSO₃⁻/Al exhibits increases in FF s ranging from 5% to 10% and the overall PCE is improved up by 19% *versus* the control devices without the quinacridone electron transporting layer (ETL). The improvement of solar cell performance can be ascribed to the increased R_{sh} (five-fold) and electron mobility (two-fold). It is worth noting that on one hand, the high-lying lowest unoccupied molecular orbital (LUMO) of Na⁺QHSO₃⁻ matches neither the LUMO of PCBM nor the work function of Al cathode, and on the other hand, the highest occupied molecular orbital (HOMO) of Na⁺QHSO₃⁻ is even higher than that of PCBM, which indicates the lack of hole-blocking ability of Na⁺QHSO₃⁻. For PSCs, the energy level matching between cathode IFL and acceptor or cathode as well as the intrinsic hole-blocking property of cathode IFL is essential. Thus, the underlying mechanism for the improved performance from Na⁺QHSO₃⁻-based cathode IFL cells deserves further investigation.

A series of small molecules containing *N,N*-diphenyl-*N,N*-bis(3-methylphenyl)-(1,1'-biphenyl)-4,4'-diamine backbone with different carboxyl side chains (Figure 9) was developed and incorporated into PSCs as anode IFLs. Three different molecules TPDA, TPDB, and TPDH (Figure 9) were synthesized and compared to the most popular anode IFL material, PEDOT:PSS, in PSCs. These solution-processable small molecules exhibit high stability and are free of post-treatment after film deposition. Moreover, the film morphology can be further controlled by varying side chain lengths. When high-performance poly[(5,6-dihydro-5-octyl-4,6-dioxo-4*H*-thieno[3,4-*c*]pyrrole-1,3-diyl)[4,8-bis[(2-ethylhexyl)oxy]benzo[1,2-*b*:4,5-*b'*]dithiophene-2,6-diyl)] (PBDTTPD) was used as the donor polymer, the resulting PSCs with the structure of ITO/TPDB/PBDTTPD:PC₆₁BM/LiF/Al showed a PCE as high as 6.51%, which was increased by ~15% *versus* the control devices. When using P3HT as the donor polymer, the highest PCE (3.03%) was achieved for the cells using TPDB IFL, which was slightly higher than that (2.94%) of the control device adopting PEDOT:PSS IFL [76]. In addition to the high PCE, the relatively high stability of TPDR-based PSCs also merit attention. Although the devices with TPDR and PEDOT:PSS IFLs show similar stability under inert condition, TPDR-based solar cells demonstrate a much slower degradation probably due to their decreased acidic and hygroscopic properties compared to PEDOT:PSS.

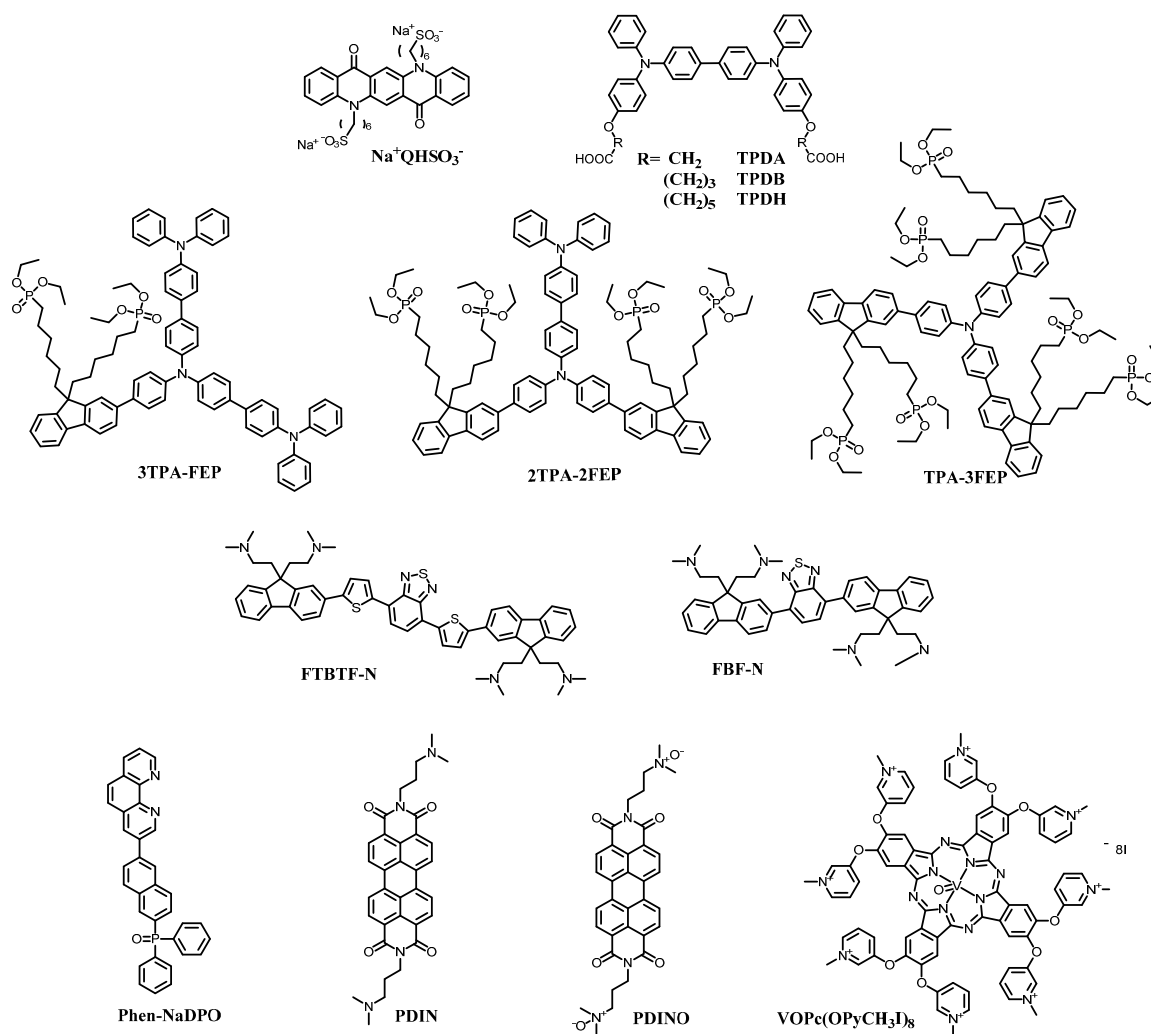


Figure 9. Chemical structures of small molecule used as interfacial layer materials for polymer solar cells.

Other triphenylamine-based alcohol-soluble small molecules featuring polar phosphonate side chains were synthesized for high-performance PSCs. Cao and coworkers reported the synthesis and application of a new series of star-like shape neutral small molecules (TPA-FEP), consisting of electron rich triphenylamine (TPA) and fluorene featuring phosphonate side chains (FEP). The series of anode IFL materials include 3TPA-FEP, 2TPA-2FEP, and TPA-3FEP as shown in Figure 9. When incorporated into PSCs with the structure of ITO/PEDOT:PSS/PCDTBT:PC₇₁BM/cathode IFL/Al, PCEs of 7.21%, 6.90%, and 6.89% were obtained for 3TPA-FEP, 2TPA-2FEP, and TPA-3FEP cells, respectively. The 7.21% PCE is among the highest for the PCDTBT PSCs. While for control device without interlayer, PCEs of 4.06% and 5.74% were obtained for the PCDTBT cells without and with methanol treatment, respectively [77]. The substantial performance enhancement for the cells using these triphenylamine IFLs can be ascribed to two factors: (1) The triphenylamine IFLs minimize the contact resistance at the active layer/cathode interface, and lead to a better ohmic contact; (2) these IFL molecules create a permanent dipole between active layer and cathode, which decreases the work function of cathode and leads to larger V_{oc} . The results indicate that water (alcohol)-soluble small molecules are promising IFL materials for PSCs.

Fang *et al.*, developed two alcohol-soluble small molecules FBF-N and FTBTF-N having different conjugated backbones as the cathode IFLs for high-performance inverted PSCs [78]. The incorporation of FBF-N or FTBTF-N (Figure 9) cathode IFL leads to an average PCE of 7.85% and 8.93% for the inverted PSCs having the device structure of ITO/BBF-N or FTBTF-N/PTB7:PC₇₁BM/MoO₃/Al, respectively, while for the control cell without cathode IFL show a substantially lower PCE of 1.18%. The introduction of the FBF-N and FTBTF-N can lead to the decrease of ITO work function by 0.3 eV. The lowered work function increases the built-in potential and facilitates electron collection, which leads to enhanced PCEs *versus* the control cells. The highest PCE of 9.22% with a J_{sc} of 17.23 mA/cm², a V_{oc} of 0.74 V, and a FF of 72.11% was obtained from PSCs containing the FTBTF-N cathode IFL. The FTBTF-N cell performance is among the highest for single junction BHJ PSCs reported to date [3,26]. In comparison to the FBF-N cells, The FTBTF-N cells show enhanced device performance due to higher J_{sc} and greater FF , which is attributed to the better phase separation and bicontinuous interpenetrating network of the active layer on FTBTF-N film than on FBF-N film induced by more hydrophobic character of FTBTF-N.

A novel IFL material (Phen-NaDPO, Figure 9) by combining triarylphosphine oxide with 1,10-phenanthroline unit was readily synthesized via Suzuki coupling and used as cathode IFL in PSCs. Phen-NaDPO dramatically decreases Ag work function from 4.62 to 2.64 eV and simultaneously improves the V_{oc} and FF in PSCs. With the device structure of ITO/PEDOT:PSS/PTB7:PC₇₁BM/ETL/cathode, the Phen-NaDPO/Ag cells show a high PCE of 7.51%, which is comparable to that (7.31%) of the device using Ca/Al cathode and outperforms that (2.19%) of the cell with Ag cathode by a big margin. When Phen-NaDPO is combined with Al cathode, the PCE of the resulting PSCs surge to 8.56% with a J_{sc} = 16.81 mA/cm², a V_{oc} = 0.75 V, and a FF = 0.68. The higher FF of devices incorporating the Phen-NaDPO cathode IFL can be attributed to the suppressed R_s and the increased R_{sh} , while the higher V_{oc} is due to the better ohmic contact between the active layer and the cathode. The work function decreasing ability of Phen-NaDPO is further investigated on both ITO and inert graphite substrate. The result shows that the work function of substrates can be reduced to

3.02 and 3.10 eV for graphite and ITO, respectively, which suggests the Phen-NaDPO potential of being a universal material to reduce work function for different substrates [79].

Recently, Wang and coworkers designed and synthesized two perylene diimide (PDI) derivative cathode IFL materials PDIN and PDINO (Figure 9), which contain amino or amino *N*-oxide (PDINO) terminal substituents on the imide, respectively [80]. PDIN and PDINO show high conductivities of 0.8×10^{-5} and 7.6×10^{-5} S/cm, respectively, which are attributed to the extended planar structure of the perylene diimide core with good self-organization characteristics. The ITO/PEDOT:PSS/PTB7:PC₇₁BM/PDINO/Al cells containing the PDI cathode IFL with widely varied thickness (10–25 nm) show promising PCEs of 8.05%–8.24%, which are substantially higher than that (4.43%) of the Al-only cells and that (6.98%) of the Ca/Al cells. The PDIN PSCs exhibit a good PCE of 7.68%. The good performance of PDIN and PDINO cells are attributed to their high conductivities, appropriate frontier molecular orbital levels, and electrode work function tuning effects. The more promising performance of PDINO-based device is attributed to the higher PDINO conductivity. It was found that the perylene diimide (PDI) interfacial layers also function well for the cells with high work function cathodes, such as Au and Ag, and for the cells using other high-performance polymer semiconductors, such as poly({4,8-bis[(5-(2-ethylhexyl)-2-thienyl]benzo[1,2-*b*:4,5-*b'*]dithiophene-2,6-diyl}{3-fluoro-2-[(2-ethylhexyl)carbonyl]thieno[3,4-*b*]thiophenediyl}) (PTB7-Th). A novel water soluble poly-*N*-alkylpyridine substituted metallophthalocyanine derivative 2,3,9,10,16,17,23,24-octakis-[*N*-methyl-(3-pyridyloxy)] vanadylphthalocyanine iodide (1:8) (VOPc(OPyCH₃I)₈) (Figure 9), namely 2,3,9,10,16,17,23,24-octakis-[*N*-methyl-(3-pyridyloxy)]vanadylphthalocyanine iodide (1:8), was synthesized as the cathode IFL for PSCs [81]. In comparison to the control cells, the PTB7:PC₇₁BM PSCs incorporating the novel cathode IFL demonstrated simultaneous enhancement of V_{oc} , J_{sc} and FF . As a result, a PCE of 8.12% for the working area of 2×2 mm² and a PCE of 7.23% for the working area of 4×4 mm² were obtained. The PCE is among the state-of-the-art performance for the PTB7:PC₇₁BM cells. The result indicates that organic molecules with poly-*N*-alkylpyridine anions should be efficient cathode IFLs for high-performance PSCs.

4. Fullerenes and Derivatives

Fullerenes and their derivatives have been widely used as electron transporting (n-type) semiconductors in bulk heterojunction films for PSCs due to their appropriate-lying frontier molecular orbitals (FMOs) and their good electron transporting capabilities. Their n-type character should render fullerenes and their derivatives as the highly promising electron transporting and hole blocking layers (or cathode IFLs) due to their structural similarity to the fullerene derivative semiconductors in the active layer, which would bridge electron transport from fullerene acceptor to cathode. Wei and coworkers first reported the usage of fullerene derivative as cathode interfacial layer for PSCs, which was formed through a spontaneous phase segregation [82]. By adding a small amount of a novel fluorinated fullerene derivative F-PCBM (Figure 10) into the P3HT:PCBM solution, the following spin-coating leads to the F-PCBM rich self-organized cathode interfacial layer induced by tailored surface energy. The generation of F-PCBM buffer layer improved the photovoltaic cell performance (3.79% PCE vs. 3.09% PCE of control cell without F-PCBM), particularly J_{sc} and FF . The performance improvement was mainly attributed to better energy level matching between PCBM and

Al cathode induced by the dipole moment of F-PCBM as well as its hole blocking property [82]. The new strategy to forming a surface-segregate IFL offers a facile and versatile approach for performance enhancement in PSCs [83]. Except for the self-organized fullerene-based IFL, a water soluble hydroxyl group containing fullerene derivative, fulleranol (Figure 10), was synthesized through a one-step procedure. The fulleranol shows excellent transparency and electron transporting capability. The incorporation of the fulleranol cathode IFL led to the P3HT:PC₆₁BM solar cells with a PCE of 3.8%, which is greater than that (3.42%) of the solar cells using ZnO cathode IFL [84]. The result demonstrates that fullerene derivatives are promising cathode IFLs for high-performance PSCs.

High-performance PSCs were fabricated using a polar fullerene derivative having carboxyl functional groups, C₆₀ pyrrolidine tris-acid (CPTA, Figure 10), as the cathode IFL layer [85]. The CPTA is soluble in methanol attributed to the polar carboxyl groups. When CPTA was incorporated into PSCs, the resulting solar cells with a structure of ITO/PEDOT:PSS/PTB7:PC₇₁BM/CPTA/Al showed a PCE of 7.92% with a J_{sc} of 16.95 mA/cm², a V_{oc} of 0.74 V, and a FF of 63%, which outperformed the control cells using Ca/Al as the cathode. In comparison to the Ca/Al cells, the J_{sc} , V_{oc} , and FF were increased simultaneously in the CPTA/Al cells. The CPTA LUMO is 3.94 eV, which lies between those of PC₇₁BM and Al and hence builds perfect energy level cascade. Thus, CPTA benefits the electron transport from PCBM to Al with suppressed energy loss, which results in enhanced PCEs.

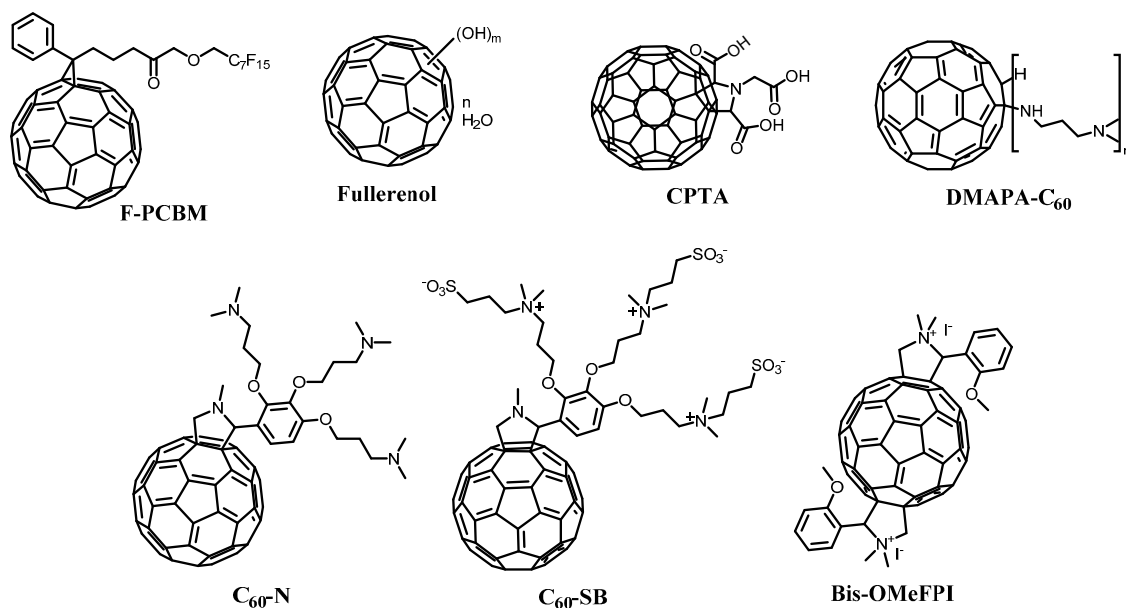


Figure 10. Chemical structures of fullerene derivative-based IFL materials F-PCBM, CPTA, DMAPA, C₆₀-N, and C₆₀-SB.

An amine group functionalized fullerene (DMAPA-C₆₀, Figure 10) was synthesized and explored as electron transporting layer in PSCs [86]. The material is readily synthesized via a simple one pot N-H addition reaction with an average addition number of ~4, which can be directly used for the device fabrication without purification. The LUMO/HOMO derived from electrochemistry is -3.58/-5.52 eV, which should ensure good electron extraction and hole blockage. In comparison to commonly used PCBM, the LUMO of DMAPA-C₆₀ is up-shifted, which is due to the addition of the

electron rich amine group. Moreover, the terminal amino group could potentially afford a dipole moment. The buffer layer can be deposited by spin-coating its methanol solution, and it was found that the active layer can be completely covered as the DMAPA-C₆₀ concentration is higher than 1 mg/mL. The incorporation of DMAPA-C₆₀ IFL led to a PCE of 3.88% for the P3HT:PCBM cells, which is 2× higher than the PCE (1.89%) for the cells without cathode IFL. The interfacial layer is also compatible with high work function cathode, such as Au, Cu, and Ag, and the resulting cells demonstrate good device performance with PCEs over 3%. When using poly(4,8-bis(5-(2-ethylhexyl)-thiophene-2-yl)-benzo[1,2-*b*:4,5-*b'*]dithiophene-*alt*-(4-(2-ethylhexanoyl)-thieno[3,4-*b*]thiophene)) (PBDTTT-C-T) as the donor polymer, the DMAPA-C₆₀/Al cells show a PCE of 7.42% with a J_{sc} of 14.83 mA/cm², a V_{oc} of 0.787 V, a FF of 62.36%, which is substantially higher than that (7.28%) of the Ca/Al cells. The results indicate that amine functionalized fullerene derivatives are promising IFLs for replacing conventional Ca cathode interfacial layer for high-performance PSCs.

Recently, Emrick and coworkers designed and synthesized two fullerene derivatives fulleropyrrolidines with tris(dimethylamino) (C₆₀-N, Figure 10) or tris(sulfobetaine) (C₆₀-SB, Figure 10) substituents as cathode IFLs for PSCs [87]. The functionalized fullerene derivatives can be readily deposited from trifluoroethanol solution and show excellent adhesion to the active layer. When incorporated into PSCs, PCEs of 9.35% ± 0.13% (maximum PCE = 9.78%) and 8.57% ± 0.15% (maximum PCE = 8.92%) were obtained for C₆₀-N/Ag and C₆₀-SB/Ag cells using PCE-10 as the donor polymer, respectively. The cells using standard Ca/Al cathode gave PCEs of 8.36% ± 0.21%. When using Al cathode, the C₆₀-N/Al and C₆₀-SB/Al cells show PCEs of 8.65% ± 0.11% and 8.29% ± 0.11%, respectively. When using high-work function metals as cathodes, the resulting C₆₀-N/Cu and C₆₀-N/Au cells also show highly efficient PCEs of 8.67% ± 0.17% and 8.56% ± 0.21%, respectively. The use of high work function metal led to improved device stability in air. Moreover, the cells using these interfacial layers afford efficient PCEs even when the film thickness is greater than 50 nm, which is significantly different from cells using conjugated polymer zwitterion IFLs, in which the interfacial layer thickness is typically less than 10 nm. The results demonstrate that the fulleropyrrolidines represent an excellent platform for electrode modification for high-performance PSCs.

Jen *et al.*, reported thermally stable and solvent resistant cathode IFL with a stable conductive fullerene doped into a thermally crosslinkable fullerene matrix for high-performance inverted PSCs [88]. The styrene was functionalized onto 1,4-di(vinylbenzyl)fullerene for crosslinking (Full-s, Figure 11) in order to maintain compact packing for high electron mobility. The bis-FPI doped and thermally crosslinked Full-x (Figure 11) film were fabricated by simple spin-coating a solution of bis-FPI and Full-S in chlorobenzene onto the ITO substrate and then subjected to thermal treatment at 210 °C, which led to a Full-x film with good solvent resistance. The *in situ* doping and crosslinking has improved both the conductivity and the solvent resistance of the resulting IFL, which leads to greatly enhanced PCE from 2.43% to 5.26% for the cells with the structure of ITO/ETL/poly(indacenodithiophene-*co*-phenanthro[9,10-*b*]quinoxaline) (PIDT-PhanQ):PC71BM/MoO₃/Ag having the optimal bis-FPI loading of 25% in the crosslinked film. For the interfacial layer with less loadings of bis-FPI, the corresponding cells show decreased J_{sc} s, FF s, and V_{oc} s (from 0.83 to 0.53 V), which is attributed to the increased interfacial resistance and the concurrently increased interfacial recombination at the cathode interfacial layer. The same group reported a new conductive fulleropyrrolidinium iodide (Bis-OMeFPI, Figure 10), which has compact ammonium and

methoxybenene groups embedded on the fullerene core [89]. The fullerene derivative can be used to dope PCBM for improving the electrical contact between active layer and ITO in inverted solar cells. When blended with a small amount of ethoxylated polyethylenimine PEIE, the conductivity of Bis-OMeFPI can be further improved with tunable work function. The derivative can be processed using orthogonal solvents for multilayer film fabrication, and its incorporation into PSCs as cathode IFL results in a very high PCE of 9.6% with a J_{sc} of 16.15 mA/cm², a V_{oc} of 0.80 V, and a FF 0.72 for the cells having the structure of ITO/Bis-OMeFPI-PEIE/poly({4,8-bis[(5-(2-ethylhexyl)-2-thienyl]benzo[1,2-*b*:4,5-*b'*]dithiophene-2,6-diyl}{3-fluoro-2-[(2-ethylhexyl)carbonyl]thieno[3,4-*b*]thiophenediyl}) (PBDTT-TT):PC₇₁BM/MoO₃/Ag [89]. The device performance was found to be insensitive to cathode IFL thickness over a wide range of 10–50 nm, which should be beneficial to large area device fabrication. The excellent performance is in good agreement with the reduced non-germinate recombination in the Bis-OMeFPI-PEIE based device *versus* the cells only using Bis-OMeFPI IFL as revealed by transient photo-voltage study. The results demonstrate the promising future of fullerene derivatives as the cathode IFLs for PSCs.

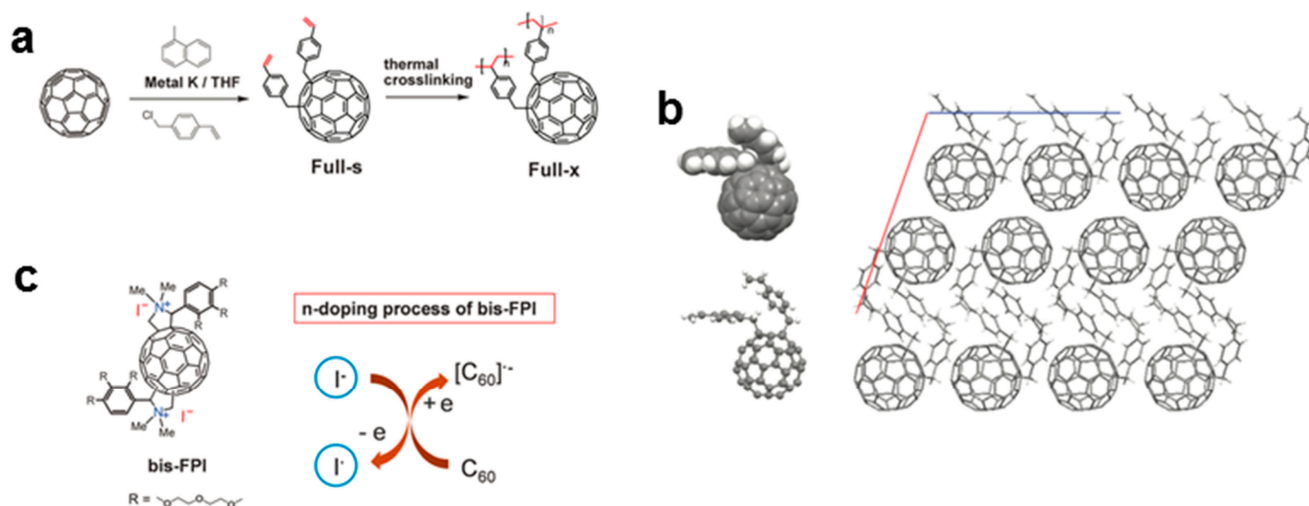


Figure 11. (a) The synthetic route to Full-s and thermally cross-linked Full-x; (b) the single crystal analysis of Full-s. Molecular packing of Full-s suggests that fullerene and vinylbenzyl groups pack in a crystalline phase; (c) the chemical structure of bis-FPI and the doping mechanism through an anion-induced electron transfer process. Reprinted with permission from [88]. Copyright 2014 Royal Society of Chemistry.

5. Graphene Oxide and Its Derivatives

Many exciting carbon-based materials have recently been investigated and incorporated into PSCs for performance enhancement and stability improvement. Among them, graphene oxide (GO) has shown great potential due to its excellent solution processability, unique two-dimensional structure, work function tunability, and good charge transporting capability. GO is graphene sheet functionalized with oxygen-containing groups in the form of epoxy and hydroxyl groups on the basal plan and various other groups, such as carboxylic acids, at the edges. The incorporation of GO IFLs has resulted in PSCs with excellent performance and good device stability [90].

Chen and coworkers firstly demonstrated the utilization of chemically derived GO thin films as hole transporting and electron blocking layer for PSCs [91]. The GO film was deposited from its neutral aqueous suspension and the deposition of GO layers serves to planarize anode surface. The work function of GO thin film was found to be 4.9 eV, and the resulting solar cells containing 2 nm thick GO showed a PCE of $3.5\% \pm 0.3\%$, which was comparable to the cells containing the conventional PEDOT:PSS anode IFL. As the GO thickness increases, the cells show degraded PCEs, which is attributed to the increased serial resistance. The device performance in combination with the simple solution-processability indicates that the GO is a highly promising hole transport and electron blocking layer in PSCs [91].

Hersam and coworkers reported a single layer of electronically tuned GO as effective replacement for PEDOT:PSS as anode IFL [92]. The GO film was deposited with a controlled density via Langmuir-Blodgett assemble, followed by low-level ozone exposure. The GO films, composed of overlapped monolayer, can be chemically tuned to achieve oxidation levels for efficient hole extraction. The GO deposition led to smooth IFL surface with an overall root-mean-square roughness of 0.7 nm. Furthermore, the GO can concurrently template a performance-optimal polymer orientation with a pi-stacked face-on microstructure (Figure 12). The resulting solar cells based on the GO anode IFL using PTB7:PC₇₁BM as the active layer showed a PCE up to 7.39%, which was comparable to the PCE (7.46%) of cells using PEDOT:PSS cathode IFL. Moreover, the GO-base cells afforded a 5× enhancement in thermal aging lifetime and a 20× enhancement in ambient lifetime *versus* analogues cells using PEDOT:PSS anode IFL.

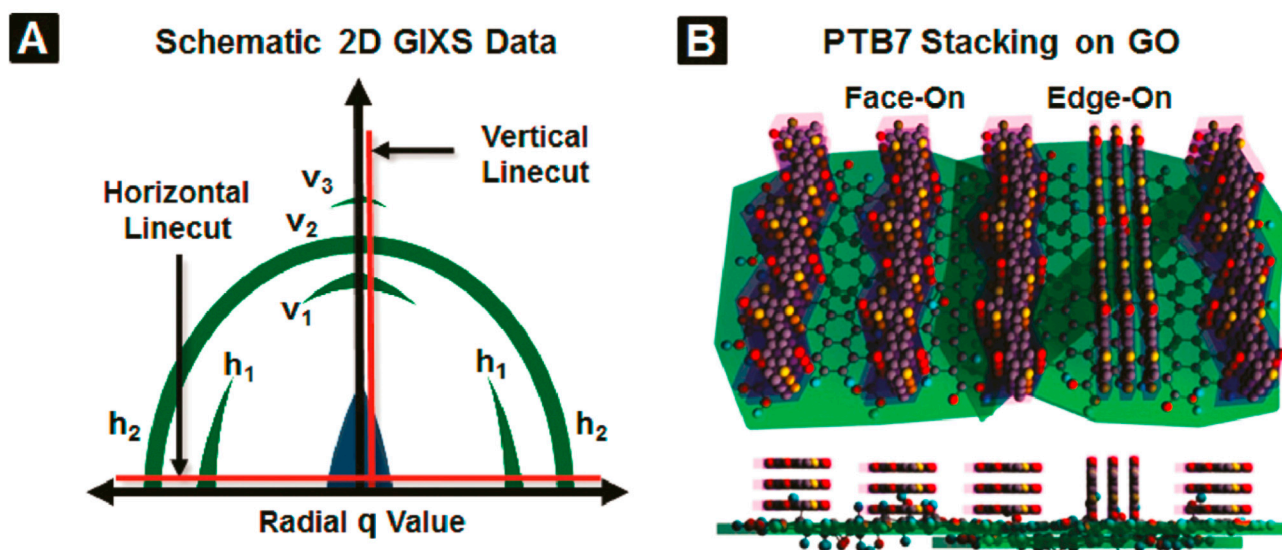


Figure 12. Grazing incidence X-ray scattering (GIXS) characterization of the microstructure of PSC active layer. (A) Schematic of raw 2D GIXS data and processing procedure for comparing signal intensities from multiple substrates, irradiated for equal times (see Supporting Information for complete 2D intensity maps); (B) Structural model from GIXS data showing preferential face-on PTB7 π -stacking on ITO/GO substrates. Reprinted with permission [92]. Copyright 2011 American Chemical Society.

Smith and coworkers recently report large area PSCs using GO anode IFL and containing PCDTBT:PC₇₁BM active layer [93]. A 2–3 nm thick GO film was deposited onto ITO substrate via spin-coating, which led to a complete coverage of GO flakes on ITO as revealed by AFM (Atomic force microscope) and SEM (Scanning electron microscope) measurement. The cells with the structure of ITO/GO/PCDTBT:P₇₀BM/BCP(or TiO_x)/Al afforded a PCE of 5%, which was comparable the performance of PSCs using PEDOT:PSS IFL. Please note that the PCEs of ~5% for the GO based devices are the highest reported for this size (0.64 cm²).

Kymakis and coworkers reported a facile, fast, non-destructive, and roll-to-roll compatible photochemical method for simultaneous reduction and doping of GO film using ultraviolet irradiation in the presence of a Cl₂ precursor gas (GO–Cl, Figure 13) [94]. It was found that the laser induced chloride atoms substitute the GO defects into both the GO edges and in the GO lattice plane. The doping and reduction level of GO–Cl can be controlled by tuning the exposure time, therefore its work function can be tailored from 4.9 to 5.23 eV, which led to a good match with HOMOs of most donors in PSCs. The PCDTBT:PC₇₁BM PSCs with GO–Cl IFL showed a PCE of 6.56%, which was 17.35% and 19.48% higher than that of the cells using pristine GO or PEDOT:PSS anode IFLs, respectively. The performance enhancement can be attributed to more efficient hole collection due to the good energy match between GO–Cl and polymer donor PCDTBT. The GO–Cl based PSCs also showed substantially higher device stability *versus* the PEDOT:PSS based cells when exposed to continuous illumination under ambient conditions.

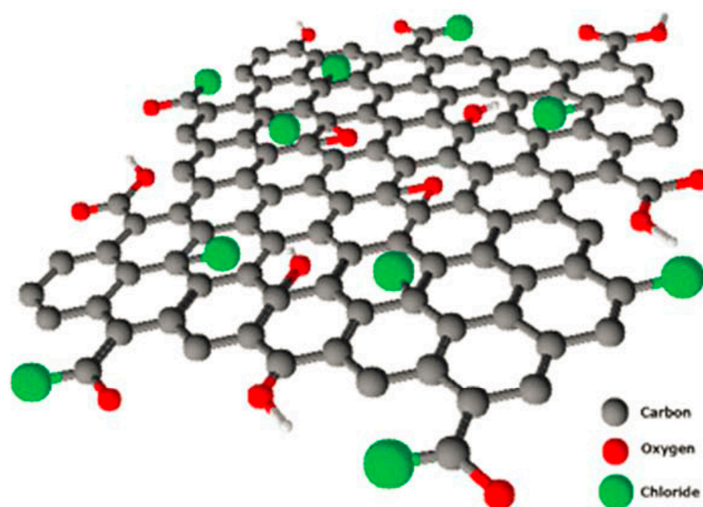


Figure 13. Chemical structure of the photo-chlorinated graphene oxide (GO–Cl) anode IFL for PSCs. Reprinted with permission from [94]. Copyright 2014 Royal Society of Chemistry.

Zhang and coworkers demonstrated similar performance enhancement for the PBDTTT–C:PC₇₁BM PSCs using chlorinated graphene oxide (Cl–GO) as anode IFL [95]. The single-layer Cl–GO sheet showed similar morphology and thickness to those of the single-layer GO sheet, and the work function of GO can be tuned by photochemical chlorination. The resulting Cl–GO showed a work function of 5.21 eV, which was aligned closely to the HOMO of polymer donor PBDTTT–C and hence led to excellent hole-extraction abilities. The PCE of PBDTTT–C:PCBM cell using chlorinated GO IFL was increased to 7.6%, which is the highest for the PBDTTT–C based cells. While, the cells using

PEDOT:PSS anode IFL only showed a PCE of 6.53%. The improved device performance is attributed to the higher photocurrent due to the maximum photo flux enabled by the high transparency of Cl-GO as well as improved hole extraction from the active layer [95]. The Cl-GO IFL also led to improved PCEs for solar cells using other active layers. The results demonstrate that the chlorinated graphene oxides should be a new class of anode IFLs for high-performance PSCs.

Other halogen-functionalized GOs were also developed for PSCs, and Na and coworkers demonstrated that fluorine-functionalized graphene oxide (FrGO) can be used as a hole transporting layer for PSCs [96]. The reduction and functionalization of GO was easily completed in one step using a novel phenylhydrazine-based reductant containing fluorine atoms, 4(trifluoromethyl)phenylhydrazine. The introduction of fluorine led to p-type doping of GO due to its high electronegativity. The PTB7:PC₇₁BM PSCs using this novel fluorinated GO IFL showed promising performance with a PCS of 6.71% with a J_{sc} of 14.84 cm²/Vs, a V_{oc} of 0.71 V, and a FF of 63.76%. The PCE was comparable to those from the cells using PEDOT:PSS IFL, but the FrGO-based solar cells showed greatly improved device stability. When using P3HT:ICBA as the active layer, the FrGO-based PSCs also exhibited similar performance enhancement *versus* PEDOT:PSS-based PSCs.

Dai and coworkers rationally designed and developed sulfated graphene oxide (GO-OSO₃H, Figure 14) with -OSO₃H groups attached on the carbon basal plane of reduced GO surrounded with edge-functionalized -COOH group [97]. The work function of sulfated GO is slightly increased from 4.7 eV of GO to 4.8 eV. The resulting GO-OSO₃H shows good work function for ohmic contact formation with the donor polymer, improved conductivity due to the reduced basal plane, and enhanced solubility attributed to the -OSO₃H/-COOH groups. The P3HT:PC₆₁BM PSCs containing GO-OSO₃H anode IFL show a greatly improved PCE of 4.37% *versus* that (3.34%) of cells using GO IFL. The performance enhancement is mainly attributed to the significantly improved FF (0.71 *vs.* 0.58), which can be attributed to the much increased conductivity of GO-SO₃H (1.3 S/m *vs.* 0.004 S/m). Moreover, the PSC performance is almost independent of the GO-OSO₃H layer thickness, which is different from the cells using insulating GO anode IFL. The result indicates that judiciously functionalized GO materials should be excellent anode IFLs in PSCs to achieve excellent device performance.

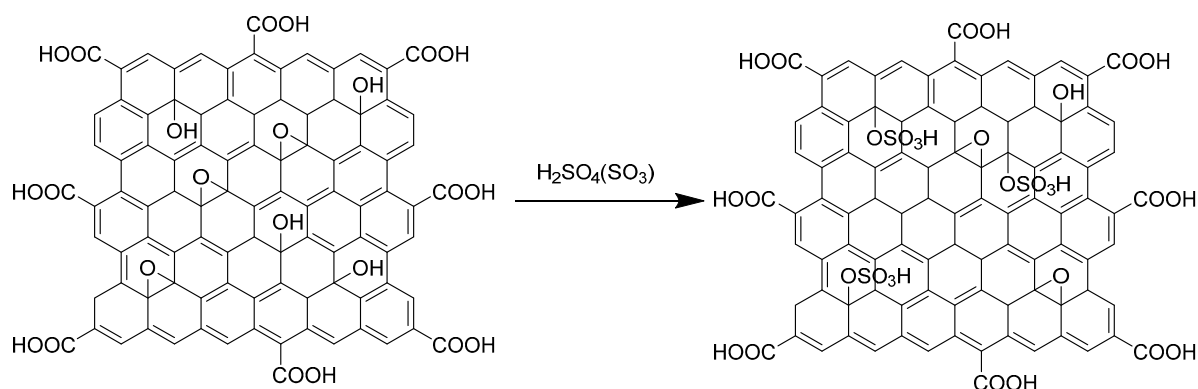


Figure 14. Synthetic Route to sulfated graphene oxide GO-OSO₃H. Reprinted with permission from [97]. Copyright 2012 American Chemical Society.

In addition to functioning as a hole transporting layer, GO derivatives can also be used as electron transporting layer. Lithium-neutralized graphene oxide (GO-Li; Figure 15) was used as an additional

layer between active layer and metal oxide cathode electron-transporting layer for PSCs. Kymakis and coworkers reported the introduction of Li to GO, and the resulting lithium-neutralized graphene oxide (GO–Li) layer can be deposited via spin-coating [98]. The replacement of H in the carboxyl group of GO with Li atoms can effectively reduce the GO WF from -4.95 to -4.27 eV (Figure 15), which led to a perfect match with the LUMO of fullerene derivatives. By incorporating the GO–Li IFL, the resulting PSCs with a device structure of ITO/PEDOT:PSS/PCDTBT:PC₇₁BM/GO–Li:TiO_x/Al showed a PCE of 6.29% with a J_{sc} of 12.51 mA/cm², a V_{oc} of 0.89 mV, and a FF of 56.5%. The PCE was increased by 14.2% in comparison to that of device without the additional graphene-based IFL. Furthermore, the GO–Li containing cells exhibited enhanced stability *versus* the cells without the interlayer, which was attributed to the shielding effects of GO–Li against humidity. Silva and coworkers reported solution processed reduced GO and metal oxide (ZnO and TiO₂) hybrid as cathode IFL for high-performance PSCs [99]. The device performance of the PSCs incorporating the nanohybrid IFL was comparable to that of cells using thermal evaporated bathocuproine (BCP) cathode IFL. The optimal PCE of 7.5% was obtained for the PTB7:PC₇₀BM cells using the nanohybrid-based IFLs, which was superior to the PCE (7.2%) of the inverted cells using only metal oxide IFLs. The reduced GO provided effective charge transfer pathways between metal oxide particles, which in combination with balanced electron and hole mobilities led to more efficient charge extraction and resulted in improved J_{sc} (14.8–15.0 mA/cm²) and FF (~65% to ~68%) [23,100].

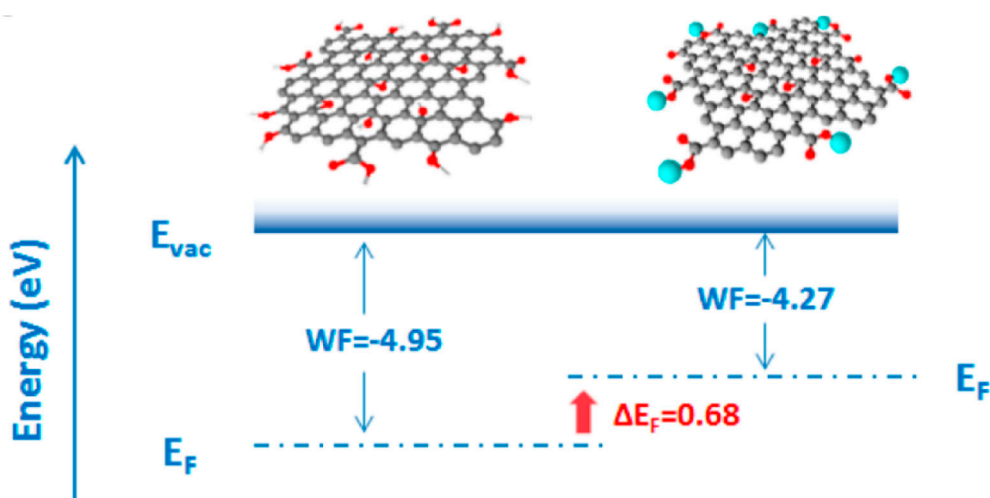


Figure 15. Energy diagram showing the Fermi level of pristine graphene oxide (GO; left) and lithium-neutralized graphene oxide (GO–Li; right). Reprinted with permission from [98]. Copyright 2014 American Chemical Society.

Heeger *et al.*, reported the synthesis of graphene having a work function of -4.6 eV by chemical vapor deposition (CVD) on copper foil. The copper foil is readily removed by etchant, and the transfer graphene thin film is prepared, which is subjected to reaction with HNO₃ to synthesize graphene oxide [101]. The resulting GO film can be directly used as electron transporting layer through stamping process (Figure 16), which leads to good contact between the GO IFL and the BHJ film. The GO cathode IFL improved the J_{sc} and PCE in PSCs, which can be attributed to the efficient charge transport and extraction from BHJ film to Al electrode. Moreover, the PCDTBT:PC₇₁BM PSCs with a cathode IFL of GO (1 nm)/TiO_x (10 nm) exhibited a PCE of 7.5% with a J_{sc} of 12.40 mA/cm², a V_{oc} of

0.88 V, and a *FF* of 0.68. The PCE is increased by 29% in comparison to that of the cells without GO IFL. The performance enhancement is attributed to the synergistic effect of improved charge transport and enhanced optical field amplitude compared to devices with single coated TiO_x or GO. The GO cells also show greatly improved device stability *versus* the TiO_x cells after storage in air for 30 days. The results indicate that graphene oxide can be effective cathode IFLs for high-performance PSCs with enhanced device durability.

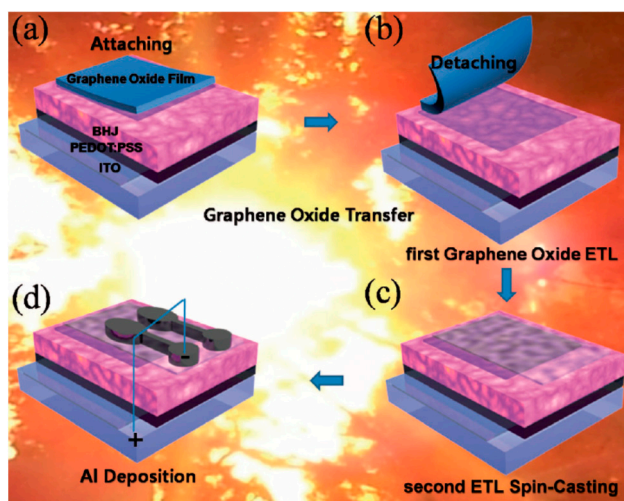


Figure 16. Schematic illustration and fabrication steps of BHJ polymer solar cells with a graphene oxide (GO) cathode IFL applied by stamping transfer. (a) Attachment of the transfer film on top of the BHJ active layer; (b) after detachment of the film, the first GO cathode IFL is uniformly transferred and coated onto the BHJ layer; (c) spin-casting of second cathode IFL of TiO_x on top of GO; (d) completed device structure after Al deposition. Reprinted with permission from [101]. Copyright 2013 Wiley-VCH Verlag GmbH & Co. KGaA.

6. Metal Oxide

Metal oxides have shown great success in improving the device performance and durability of PSCs. Among them, TiO_x and ZnO are the two most widely studied cathode IFLs, and their incorporations have greatly improved the PCEs of PSCs. In the meantime, they can act as diffusion barriers against oxygen and water attributed to their scavenging effects originating from photocatalysis and oxygen defects. Processing or fabricating TiO_x IFL at low temperature is a highly favorable method for practical applications, but the resulting film typically shows low electron mobility, which limits the charge transport and collection, hence leading to low PCEs. Thermal annealing at temperatures above 400 °C can convert the amorphous film to crystalline film, and hence greatly improve its charge transport properties. Due to the significant effect of film microstructure and crystallinity on charge transport properties, a great deal of research efforts has been devoted to development of effective film deposition methods to control these properties.

As n-type semiconductor, TiO₂ was a promising candidate as an electron acceptor and transport materials for hybrid polymer/TiO₂ solar cells [102,103]. Song *et al.* [104] used TiO₂ as n-type semiconductor in hybrid solar cells [105] with a device structure of ITO/TiO₂/MEHPPV/PEDOT/Au.

The TiO_2 functions not only as electron acceptor layer but also as hole blocking IFL, however the resulting PSCs show a limited PCE of 0.51% [104]. Kim and coworkers introduced a thin layer TiO_x as optical spacer for re-distributing the light intensity inside the solar cell (Figure 17), which leads to highly efficient PCEs in PSCs [106]. The pioneering work of Kim greatly promotes the usage of TiO_x as IFL in PSCs. A solution based sol-gel process was employed to fabricate TiO_x layer on the top of the polymer:PCBM active layer. The TiO_x film was deposited using a TiO_x precursor solution, which was followed by hydrolysis in air at room temperature (Figure 17b). The film was then reacted at 150 °C for 10 min inside a glovebox. Film characterization indicates that the resulting film is amorphous and has an oxygen deficiency at the surface. Using the TiO_x as the cathode IFL, the P3HT:PCBM cells showed substantial enhancement of ~40% in the incident photon-to-current collection efficiency (IPCE) over entire excitation spectral range *versus* the cells without using TiO_x layer. The enhanced absorption was attributed to the result of the TiO_x optical spacer effect (Figure 17a), which led to a greatly improved PCE of 5.0% *versus* the PCE of 2.3% from the cells without TiO_x IFL. The effect of TiO_x on increasing the PSC performance has also been demonstrated by the same group using other active layers, and the PCDTBT:PC₇₀BM solar cells showed an internal quantum efficiency (IQE) approaching 100% round 500 nm with a certified PCE of 5.96% under AM 1.5 irradiation [38]. The ~100% IQE implies that almost absorbed photon leads to a separated pair of charge carriers, which is collected at the electrode. The results demonstrate that TiO_x is an excellent cathode IFL and provides optical space for high-performance PSCs.

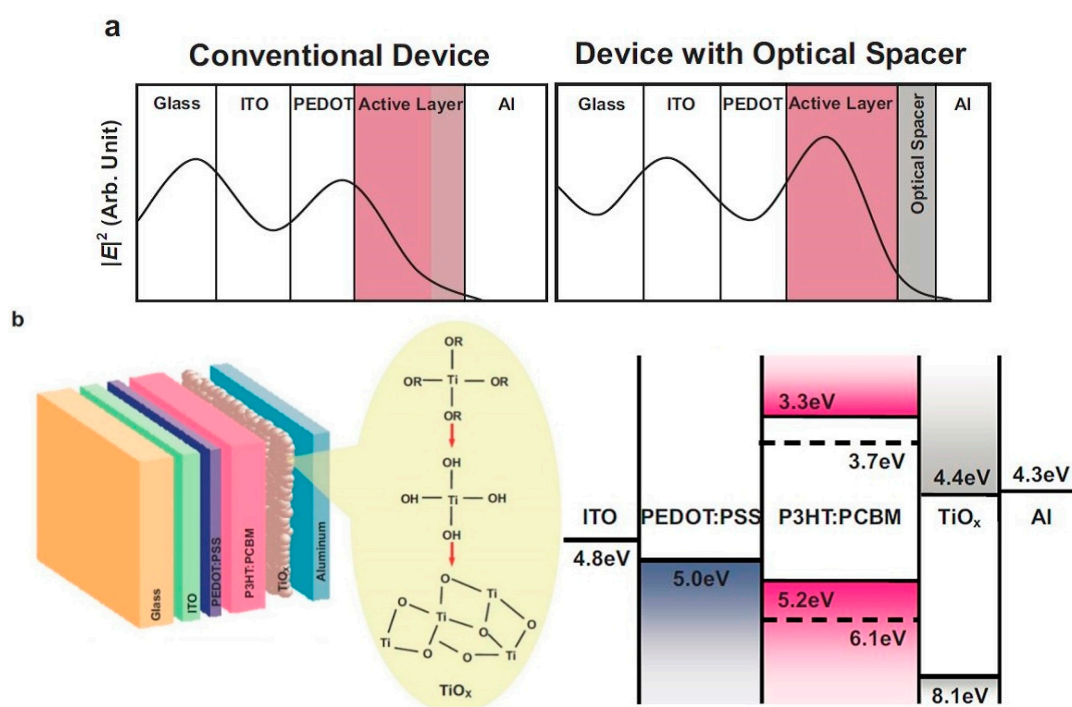


Figure 17. (a) Schematic illustration of the squared spatial electric field, $|E|^2$, spatial distribution inside the solar cells with a structure of ITO/PEDOT/active layer/Al (left) and ITO/PEDOT/active layer/optical spacer/Al (right); (b) Schematic illustration of the device structure (left) with a brief synthetic route to the TiO_x interfacial layer and the energy level diagram (right) of the single components of the polymer solar cells. Reprinted with permission from [106]. Copyright 2006 Wiley-VCH Verlag GmbH & Co. KGaA.

Later, Yang and coworkers developed a novel approach for fabricating high-performance PSCs by introducing dopants into metals oxide IFLs [107]. The Cs doped TiO₂ is prepared via adding Cs₂CO₃ solution to the nanocrystalline TiO₂ solution. In addition to the stable nanostructure morphology of TiO₂:Cs IFL, The TiO₂ doped with Cs leads to more favored work function for charge collection, and the conventional P3HT:PC₇₁BM solar cells using the Cs doped TiO₂ cathode IFL show an excellent PCE up to 4.2% *versus* the PCE of 2.4% from the cells using TiO₂ IFL. The performance enhancement for the TiO₂:Cs cells is attributed to the more efficient electron extraction and hole blocking property of the TiO₂ interfacial layer. Choy and coworkers reported enhanced electron extraction by incorporating metal nanoparticle into the TiO₂ cathode IFL [40]. The Au and Ag nanoparticles are embedded in titanium oxide (TiO₂) layer, and the resulting PSCs show a PCE reaching 8.2% with a J_{sc} of 16.21 mA/cm², a V_{oc} of 0.787 V, and a FF of 64.3%. The performance enhancement is mainly attributed to reduced charge transport resistance and, hence, excellent charge extraction and collection at the electrode.

ZnO is another excellent solution-processable cathode IFL for PSCs. In addition to the good transparency and the effective hole blocking effect, the film of ZnO nanoparticle has a high electron mobility of ~0.1 cm²/Vs, which is greatly larger than that of TiO_x film [108]. The application of ZnO as cathode IFL was pioneered by Shirakawa in 2004 [109]. The incorporation of the sputter-deposited ZnO IFL affords a PCE of 1.0% for the bilayer cell having a structure of ITO/ZnO/C₆₀/P3HT/Au under illumination of 100 mW/cm². Later, White *et al.*, demonstrated non-vacuum, solution processed ZnO IFL for efficient PSCs. The ZnO buffer layer was fabricated from a zinc acetate solution in 96% 2-methoxyethanol and 4% ethanolamine after thermal annealing at 300 °C in air. The ITO/ZnO/P3HT:PCBM/Ag inverted BHJ solar cells show a promising PCE of 2.97% [110]. Since then, various methods have been developed to deposit ZnO thin film. Among them, sol-gel approach has been extensively used as the solution-based thin film deposition technique, which is highly suitable for the fabrication of inverted solar cells. However, a high thermal annealing temperature is typically needed in the sol-gel method to promote film crystallinity and to remove the residual organic compounds, which should not be compatible for the fabrication of flexible solar cells. Solution-processed ZnO nanoparticle via spin-coating has also been developed for film deposition. Using the spin-coated ZnO cathode IFL annealed at 200 °C in air, So and coworkers reported inverted PDTG-TPD:PC₇₁BM solar cells with a promising average PCE of 7.3% [111]. The results demonstrate the promising potentials of ZnO as cathode IFL.

It is known that up to ~30% of the atomic bonds in ZnO nanoparticles are dangling bonds, which can lead to high degree of charge recombination and result in low PCEs for the corresponding PSCs. It was found that further treatment of ZnO nanoparticle IFL with UV-ozone (UVO) can passivate the defect states. Oxygen vacancy concentration was reduced by oxygen penetration in the nanoparticle films; therefore, defects in ZnO nanoparticles were passivated by UVO treatment, which led to longer charge carrier lifetime and reduced interface recombination *versus* the cells treated with only light soaking [112]. The ZnO nanoparticle films were exposed to UV light at 254 nm after thermal annealing at 80 °C, and the resulting poly(thieno[3,4-*c*]pyrrole-4,6-dione-*co*-dithienosilole) (PDTs-TPD) and poly(thieno[3,4-*c*]pyrrole-4,6-dione-*co*-dithienogermole) (PDTG-TPD) cells having the structure ITO/ZnO nanoparticles/polymer:PC₇₁BM/MoO₃/Ag show a further improved average PCEs of 7.8% and 8.1%, respectively [112].

Heeger and coworkers developed a low temperature (≤ 200 °C) annealed sol-gel derived ZnO film as the cathode IFL for PSCs [113]. A zinc acetate in 2-methoxyethanol was used as the precursor solution, which was spin-coated onto ITO substrate and subsequently subjected to thermal treatment at different temperatures (130, 150, and 200 °C) for 1 h. The precursor was converted to dense ZnO film by hydrolysis. The ultraviolet photoelectron spectroscopy (UPS)-derived conduction band minimum was found to be 4.33 ± 0.07 eV, which should lead to a good match with the LUMO (3.6 eV) of PC₇₀BM. The PCDTBT:PC₇₀BM solar cells using the sol-gel derived ZnO cathode IFL after annealing at 200 °C showed a PCE of 6.33% with a J_{sc} of 10.41 mA/cm², a V_{oc} of 0.88 V, and a FF of 68.8%. A comparable PCE of 6.03% was obtained for the cells using the ZnO IFL annealed at 150 °C, however, the cells with ZnO annealed at 130 °C showed a reduced PCE of 5.36% with a lower J_{sc} , a smaller V_{oc} , and a higher series resistance (R_s). In comparison to the high annealing temperature required in the previous methods [114], the temperature used for the thermal treatment in the Heeger's approach is relatively low, which should be compatible with flexible substrates. Moreover, the incorporation of ZnO IFL leads to the resulting PSCs with good device stability, and the PCE remains above 70% of its original value after storage at ambient conditions for 30 days. The low annealing temperature (≤ 200 °C) used to grow the ZnO IFL affords a promising pathway to fabricate PSCs with high-performance and long-term stability [45].

Using sol-gel derived ZnO cathode IFL and employing inverted structure, Marks and coworkers reported PSCs with unprecedented FF s approaching 80% using highly ordered polymer donor semiconductors. Film morphology characterization (Figure 18) revealed that the polymer:PCBM active layer has achieved vertical phase degradation with PCBM enrichment on the ZnO surface and polymer enrichment on the active layer/air interface. Such morphology arises from the surface energy difference between the polymer and PC₇₁BM, and their interaction with ZnO IFL [23]. Moreover, the ZnO interface can template close π -stacking with a face-on orientation, which facilitates charge extraction and suppresses charge recombination, which in combination with the high mobility of the polymer leads to exceptionally high FF s. Therefore, the interfacial layer not only selectively collects charge carriers, but also greatly affects the morphologies of the active layer deposited onto it.

In addition to ZnO IFL, ZnO-based hybrid IFL was also developed as cathode IFL for high-performance PSCs. So and coworker reported the incorporation of surface-modified ZnO–poly(vinyl pyrrolidone) (PVP) nanocomposite as electron-transporting IFL [100]. In comparison to traditional sol-gel ZnO IFL, the ZnO–PVP nanocomposite could have more uniformly distributed ZnO nanocluster in the polymer matrix by suppressing ZnO nanocluster aggregation. The nanocomposite IFL was prepared from Zinc acetate and PVP solution in ethanol, which is stabilized by ethanolamine. UV-ozone treatment of the nanocomposite resulted in enhanced J_{sc} s and FF s for poly(thieno[3,4-*c*]pyrrole-4,6-dione-*co*-dithienogermole) (PDTG–TPD):PC₇₁BM inverted cells compared to those from the cells using as-prepared IFL films. Optimal cells were obtained after 10 min UV-ozone treatment to remove PVP polymer at the ZnO-PVP nanocomposite surface and showed a remarkable PCE of 8.1% with a J_{sc} of 14.0 mA/cm², a V_{oc} of 0.86 V, and a FF of 67.3% under AM 1.5G illumination at 100 mW/cm². The enhanced performance of ITO/ZnO-PVP nanocomposite/PDTG–TPD:PC₇₁BM/MoO₃/Ag cells was attributed to the modified surface composition, which promoted charge collection due to better electronic coupling between the ZnO nanocluster within the nanocomposite IFL and PC₇₁BM in the active layer. The device fabrication developed by So is compatible with the large scale roll-to-roll process.

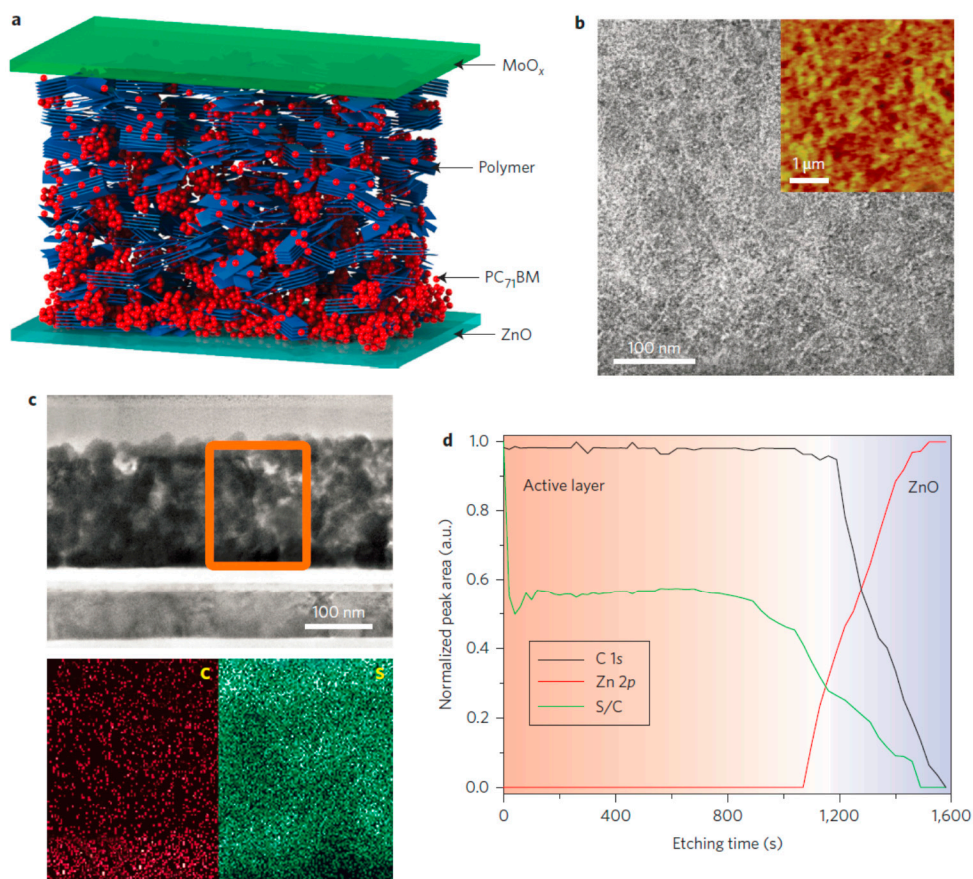


Figure 18. Morphology of an inverted PSC using ZnO cathode IFL, which yields optimal performance. **(a)** Schematic of the PBTI3T:PC₇₁BM blend film showing vertical phase gradation with a polymer-rich layer near the MoO_x/blend interface and a PC₇₁BM-rich layer near the blend/ZnO interface; **(b)** TEM (Transmission electron microscopy) image of a PBTI3T:PC₇₁BM blend film. Inset: AFM topographical image; **(c)** TEM cross-sectional image and EDS C and S element mappings of an optimized PBTI3T:PC₇₁BM inverted PSC. EDS mappings were performed simultaneously on the TEM cross-sectional sample across the active layer; **(d)** XPS depth profile of a PBTI3T:PC₇₁BM blend film showing S:C ratio evolution as a function of etching time, where etching begins at the air/film interface. Reprinted with permission from [23]. Copyright 2013, Rights Managed by Nature Publishing Group.

In addition to functioning as cathode IFL, metal oxide can also be used as anode IFL for PSCs. NiO was known to be a p-type semiconductor. The p-type conductivity originates from two positively charged holes which accompany each Ni²⁺ vacancy in the lattice for charge neutrality [115]. The large work function of NiO allows a good match between its valence band and the HOMO of the most of polymer donors. Marks and coworkers reported the incorporation of a thin layer (5–10 nm) of NiO between the P3HT:PCBM active layer and ITO anode in PSCs [116]. The NiO film was deposited by pulsed laser deposition (PLD). The resulting cells with a structure of ITO/NiO/P3HT:PCBM/LiF/Al afford a dramatically enhanced PCE of 5.2% with a high *FF* of 69% and a substantial *V*_{oc} of 0.64 V *versus* the PEDOT:PSS control cells. The performance enhancement of NiO-based cells is attributed to

the favorable energy band alignment, interface passivation, crystallinity, smooth surface, and optical transparency of NiO IFL [117]. The results indicate that NiO is an excellent p-type semiconductor as anode IFL for high-performance PSCs [118].

In addition to pulsed laser deposition, NiO_x is also compatible with solution-based processing techniques, and Olso *et al.*, reported an easily implemented solution-processed NiO_x anode IFL for high-performance PSCs. The NiO_x IFL was deposited by spin-coating Ni precursor ink followed by thermal annealing at 300 °C for 1 h. The work function of ITO modified with a solution-processed NiO_x matches well with the ionization potential of the donor semiconductor PCDTBT in the BHJ film. Oxygen plasma treatment of NiO_x anode IFL is shown to provide superior contact with the donor semiconductors having high ionization potentials by increasing the ITO/NiO_x work function by 0.500 eV as revealed by photoemission spectroscopy measurements. The conduction band of NiO_x is 2.1 eV, which allows NiO_x to serve as an effective electron blocking layer to suppress charge recombination at electrodes. The incorporation of NiO_x IFL leads to the resulting PSCs with an improved diode ideal factor n and a 10^3 reduction of J_{sat} . The cells having a structure of ITO/NiO_x/PCDTBT:PC₇₁BM/Ca/Al show a PCE of 6.7%, which is increased by 17.3% *versus* the PCE (5.7%) of the cells using PEDOT:PSS IFL [119]. So and coworkers reported a similar device performance enhancement employing solution processable NiO IFL [120]. The nickel acetate tetrahydrate and monoethanolamine in an ethanolic solution was chosen as the precursor solution, which can be thermally converted to form non-stoichiometric p-type NiO. The PDTG-TPD:PC₇₁BM cells using this NiO IFL with 5 nm thickness show an average PCE of 7.8% with a J_{sc} of 13.9 mA/cm², a V_{oc} of 0.82 V, and a FF of 68.4%, which outperform the cells by 15% using PEDOT:PSS IFL. The performance enhancement was attributed to the optical resonance and more homogeneous donor/acceptor active layer morphology induced by hydrophobic NiO. Moreover, the devices incorporating the NiO anode IFL show better device stability in air *versus* the cells using PEDOT:PSS IFL.

7. Other Interfacial Layer Materials

In addition to aforementioned IFL materials types, some other classes of materials have also been developed and incorporated into PSCs, mainly including self-assembly monolayers (SAMs) [121–124], crosslinked semiconducting blends [125,126], multifunctional quantum-dot monolayers [127], and inorganic salts [128]. As emerging IFLs for polymer solar cells, these materials have shown some promising characteristics for performance enhancement and stability improvement. However, the optimal performance of the PSCs incorporating these novel IFLs is still lower than those of the cells incorporating well-studied IFLs discussed above. However, as emerging IFL materials they offer great opportunities for organic solar cells, further understanding fundamental IFL operation mechanisms, and material development and optimization will deliver more promising device performance in the near future.

8. Conclusions

In summary, we have reviewed five types of interfacial layer materials for applications in high-performance polymer solar cells, and the device performance of resulting cells has been discussed with respect to the function and operation mechanisms of these interfacial layers. The interfacial layer

engineering has shown significant impacts on achieving high power conversion efficiency cells with robust device operation stability in the last decade. By incorporating novel interfacial layers with fine-tuned optical and electrical properties, the resulting solar cells have recently shown power conversion efficiencies greater than 10%. Appropriate interfacial layers can maximize the open-circuit voltages of the resulting solar cells by promoting ohmic contact formation and the interfacial layer can also significantly increase short-circuit voltages and fill factors by optimizing solar absorption and suppressing charge carrier recombination. Other important beneficial effects have also been observed; the interfacial layers can alter the active layer film morphology. Active layers with vertical phase separation have been achieved through surface energy engineering. Interfacial layer engineering enables us to adopt electrodes with high work function, which in combination with the kinetic barrier against water and oxygen penetration, can lead to increased device air stability. Although interfacial layers have made a significant contribution to the device performance improvement in polymer solar cells in the last decade, there is great room for performance enhancement. By designing interfacial layer materials with fine-tuned electronic, electrical, optical and chemical properties to minimize the performance loss, more promising polymer solar cells with robust device stability should be developed in the near future.

Acknowledgments

We thank the Shenzhen Basic Research Fund (JCYJ20140714151402769) and SUSC start-up fund for providing financial support during the time this review was written.

Author Contributions

All authors are involved in literature search and manuscript preparation.

Conflicts of Interest

The authors declare no conflict of interest.

References

1. Coakley, K.M.; McGehee, M.D. Conjugated polymer photovoltaic cells. *Chem. Mater.* **2004**, *16*, 4533–4542.
2. Günes, S.; Neugebauer, H.; Sariciftci, N.S. Conjugated polymer-based organic solar cells. *Chem. Rev.* **2007**, *107*, 1324–1338.
3. Guo, X.; Facchetti, A.; Marks, T.J. Imide- and amide-functionalized polymer semiconductors. *Chem. Rev.* **2014**, *114*, 8943–9021.
4. Krebs, F.C. Fabrication and processing of polymer solar cells: A review of printing and coating techniques. *Sol. Energy Mater. Sol. Cells* **2009**, *93*, 394–412.
5. Krebs, F.C.; Gevorgyan, S.A.; Alstrup, J. A roll-to-roll process to flexible polymer solar cells: Model studies, manufacture and operational stability studies. *J. Mater. Chem.* **2009**, *19*, 5442–5451.

6. Søndergaard, R.R.; Hösel, M.; Krebs, F.C. Roll-to-roll fabrication of large area functional organic materials. *J. Polym. Sci. B Polym. Phys.* **2013**, *51*, 16–34.
7. Zhou, N.; Buchholz, D.B.; Zhu, G.; Yu, X.; Lin, H.; Facchetti, A.; Marks, T.J.; Chang, R.P.H. Ultraflexible polymer solar cells using amorphous zinc–indium–tin oxide transparent electrodes. *Adv. Mater.* **2014**, *26*, 1098–1104.
8. Zhao, B.; He, Z.; Cheng, X.; Qin, D.; Yun, M.; Wang, M.; Huang, X.; Wu, J.; Wu, H.; Cao, Y. Flexible polymer solar cells with power conversion efficiency of 8.7%. *J. Mater. Chem. C* **2014**, *2*, 5077–5082.
9. Coughlin, J.E.; Henson, Z.B.; Welch, G.C.; Bazan, G.C. Design and synthesis of molecular donors for solution-processed high-efficiency organic solar cells. *Acc. Chem. Res.* **2013**, *47*, 257–270.
10. Chen, Y.; Wan, X.; Long, G. High performance photovoltaic applications using solution-processed small molecules. *Acc. Chem. Res.* **2013**, *46*, 2645–2655.
11. Harschneck, T.; Zhou, N.; Manley, E.F.; Lou, S.J.; Yu, X.; Butler, M.R.; Timalina, A.; Turrisi, R.; Ratner, M.A.; Chen, L.X.; *et al.* Substantial photovoltaic response and morphology tuning in benzo[1,2-*b*:6,5-*b'*]dithiophene (bBDT) molecular donors. *Chem. Commun.* **2014**, *50*, 4099–4101.
12. Liang, Y.; Yu, L. A new class of semiconducting polymers for bulk heterojunction solar cells with exceptionally high performance. *Acc. Chem. Res.* **2010**, *43*, 1227–1236.
13. Ye, L.; Zhang, S.; Huo, L.; Zhang, M.; Hou, J. Molecular design toward highly efficient photovoltaic polymers based on two-dimensional conjugated benzodithiophene. *Acc. Chem. Res.* **2014**, *47*, 1595–1603.
14. Zhou, N.; Lin, H.; Lou, S.J.; Yu, X.; Guo, P.; Manley, E.F.; Loser, S.; Hartnett, P.; Huang, H.; Wasielewski, M.R.; *et al.* Morphology-performance relationships in high-efficiency all-polymer solar cells. *Adv. Energy Mater.* **2014**, *4*, doi:10.1002/aenm.201300785.
15. Guo, X.; Zhou, N.; Lou, S.J.; Hennek, J.W.; Ponce Ortiz, R.; Butler, M.R.; Boudreault, P.-L.T.; Strzalka, J.; Morin, P.-O.; Leclerc, M.; *et al.* Bithiopheneimide–dithienosilole/dithienogermole copolymers for efficient solar cells: Information from structure–property–device performance correlations and comparison to thieno[3,4-*c*]pyrrole-4,6-dione analogues. *J. Am. Chem. Soc.* **2012**, *134*, 18427–18439.
16. Hartnett, P.E.; Timalina, A.; Matte, H.S.S.R.; Zhou, N.; Guo, X.; Zhao, W.; Facchetti, A.; Chang, R.P.H.; Hersam, M.C.; Wasielewski, M.R., *et al.* Slip-stacked perylenediimides as an alternative strategy for high efficiency nonfullerene acceptors in organic photovoltaics. *J. Am. Chem. Soc.* **2014**, *136*, 16345–16356.
17. Thompson, B.C.; Fréchet, J.M.J. Polymer–fullerene composite solar cells. *Angew. Chem. Int. Ed.* **2008**, *47*, 58–77.
18. Yu, G.; Gao, J.; Hummelen, J.C.; Wudl, F.; Heeger, A.J. Polymer photovoltaic cells-enhanced efficiencies via a network of internal donor-acceptor heterojunctions. *Science* **1995**, *270*, 1789–1791.
19. Halls, J.J.M.; Walsh, C.A.; Greenham, N.C.; Marseglia, E.A.; Friend, R.H.; Moratti, S.C.; Holmes, A.B. Efficient photodiodes from interpenetrating polymer networks. *Nature* **1995**, *376*, 498–500.

20. Cheng, Y.-J.; Yang, S.-H.; Hsu, C.-S. Synthesis of conjugated polymers for organic solar cell applications. *Chem. Rev.* **2009**, *109*, 5868–5923.
21. Guo, X.; Watson, M.D. Pyromellitic diimide-based donor–acceptor poly(phenylene ethynylene)s. *Macromolecules* **2011**, *44*, 6711–6716.
22. Peet, J.; Heeger, A.J.; Bazan, G.C. “Plastic” solar cells: Self-assembly of bulk heterojunction nanomaterials by spontaneous phase separation. *Acc. Chem. Res.* **2009**, *42*, 1700–1708.
23. Guo, X.; Zhou, N.; Lou, S.J.; Smith, J.; Tice, D.B.; Hennek, J.W.; Ortiz, R.P.; Navarrete, J.T.L.; Li, S.; Strzalka, J.; *et al.* Polymer solar cells with enhanced fill factors. *Nat. Photon.* **2013**, *7*, 825–833.
24. Xin, H.; Guo, X.; Ren, G.; Watson, M.D.; Jenekhe, S.A. Efficient phthalimide copolymer-based bulk heterojunction solar cells: How the processing additive influences nanoscale morphology and photovoltaic properties. *Adv. Energy Mater.* **2012**, *2*, 575–582.
25. You, J.; Dou, L.; Yoshimura, K.; Kato, T.; Ohya, K.; Moriarty, T.; Emery, K.; Chen, C.-C.; Gao, J.; Li, G.; *et al.* A polymer tandem solar cell with 10.6% power conversion efficiency. *Nat. Commun.* **2013**, *4*, doi:10.1038/ncomms2411.
26. He, Z.; Zhong, C.; Su, S.; Xu, M.; Wu, H.; Cao, Y. Enhanced power-conversion efficiency in polymer solar cells using an inverted device structure. *Nat. Photon.* **2012**, *6*, 591–595.
27. Liu, Y.; Zhao, J.; Li, Z.; Mu, C.; Ma, W.; Hu, H.; Jiang, K.; Lin, H.; Ade, H.; Yan, H. Aggregation and morphology control enables multiple cases of high-efficiency polymer solar cells. *Nat. Commun.* **2014**, *5*, doi:10.1038/ncomms6293.
28. Chen, J.-D.; Cui, C.; Li, Y.-Q.; Zhou, L.; Ou, Q.-D.; Li, C.; Li, Y.; Tang, J.-X. Single-junction polymer solar cells exceeding 10% power conversion efficiency. *Adv. Mater.* **2014**, 1035–1041.
29. Huang, Y.; Kramer, E.J.; Heeger, A.J.; Bazan, G.C. Bulk heterojunction solar cells: Morphology and performance relationships. *Chem. Rev.* **2014**, *114*, 7006–7043.
30. Kearns, D.; Calvin, M. Photovoltaic effect and photoconductivity in laminated organic systems. *J. Chem. Phys.* **1958**, *29*, 950–951.
31. Tang, C.W. Two-layer organic photovoltaic cell. *Appl. Phys. Lett.* **1986**, *48*, 183–185.
32. Wei, G.; Xiao, X.; Wang, S.; Zimmerman, J.D.; Sun, K.; Diev, V.V.; Thompson, M.E.; Forrest, S.R. Arylamine-based squaraine donors for use in organic solar cells. *Nano Lett.* **2011**, *11*, 4261–4264.
33. Lin, Y.; Ma, L.; Li, Y.; Liu, Y.; Zhu, D.; Zhan, X. Small-molecule solar cells with fill factors up to 0.75 via a layer-by-layer solution process. *Adv. Energy Mater.* **2014**, *4*, doi:10.1002/aenm.201300626.
34. Guo, X.; Marks, T.J. Plastic solar cells with engineered interfaces. *Proc. SPIE* **2013**, *2013*, doi:10.1117/12.2013491.
35. Po, R.; Carbonera, C.; Bernardi, A.; Camaioni, N. The role of buffer layers in polymer solar cells. *Energy Environ. Sci.* **2011**, *4*, 285–310.
36. Steim, R.; Kogler, F.R.; Brabec, C.J. Interface materials for organic solar cells. *J. Mater. Chem.* **2010**, *20*, 2499–2512.
37. Lai, T.-H.; Tsang, S.-W.; Manders, J.R.; Chen, S.; So, F. Properties of interlayer for organic photovoltaics. *Mater. Today* **2013**, *16*, 424–432.

38. Park, S.H.; Roy, A.; Beaupre, S.; Cho, S.; Coates, N.; Moon, J.S.; Moses, D.; Leclerc, M.; Lee, K.; Heeger, A.J. Bulk heterojunction solar cells with internal quantum efficiency approaching 100%. *Nat. Photon.* **2009**, *3*, 297–302.
39. Li, X.; Choy, W.C.H.; Huo, L.; Xie, F.; Sha, W.E.I.; Ding, B.; Guo, X.; Li, Y.; Hou, J.; You, J.; *et al.* Dual plasmonic nanostructures for high performance inverted organic solar cells. *Adv. Mater.* **2012**, *24*, 3046–3052.
40. Xie, F.-X.; Choy, W.C.H.; Sha, W.E.I.; Zhang, D.; Zhang, S.; Li, X.; Leung, C.-W.; Hou, J. Enhanced charge extraction in organic solar cells through electron accumulation effects induced by metal nanoparticles. *Energy Environ. Sci.* **2013**, *6*, 3372–3379.
41. Xiao, Z.; Yuan, Y.; Yang, B.; VanDerslice, J.; Chen, J.; Dyck, O.; Duscher, G.; Huang, J. Universal formation of compositionally graded bulk heterojunction for efficiency enhancement in organic photovoltaics. *Adv. Mater.* **2014**, *26*, 3068–3075.
42. Jørgensen, M.; Norrman, K.; Gevorgyan, S.A.; Tromholt, T.; Andreasen, B.; Krebs, F.C. Stability of polymer solar cells. *Adv. Mater.* **2012**, *24*, 580–612.
43. Zhou, Y.; Fuentes-Hernandez, C.; Shim, J.; Meyer, J.; Giordano, A.J.; Li, H.; Winget, P.; Papadopoulos, T.; Cheun, H.; Kim, J.; *et al.* A universal method to produce low-work function electrodes for organic electronics. *Science* **2012**, *336*, 327–332.
44. Reese, M.O.; Morfa, A.J.; White, M.S.; Kopidakis, N.; Shaheen, S.E.; Rumbles, G.; Ginley, D.S. Pathways for the degradation of organic photovoltaic P3HT:PCBM based devices. *Sol. Energy Mater. Sol. Cells* **2008**, *92*, 746–752.
45. Zhou, N.; Guo, X.; Ortiz, R.P.; Li, S.; Zhang, S.; Chang, R.P.H.; Facchetti, A.; Marks, T.J. Bithiophene imide and benzodithiophene copolymers for efficient inverted polymer solar cells. *Adv. Mater.* **2012**, *24*, 2242–2248.
46. Gomez, E.D.; Loo, Y.-L. Engineering the organic semiconductor-electrode interface in polymer solar cells. *J. Mater. Chem.* **2010**, *20*, 6604–6611.
47. Roman, L.S.; Mammo, W.; Pettersson, L.A.A.; Andersson, M.R.; Inganäs, O. High quantum efficiency polythiophene. *Adv. Mater.* **1998**, *10*, 774–777.
48. Scott, J.C.; Malliaras, G.G.; Chen, W.D.; Breach, J.-C.; Salem, J.R.; Brock, P.J.; Sachs, S.B.; Chidsey, C.E.D. Hole limited recombination in polymer light-emitting diodes. *Appl. Phys. Lett.* **1999**, *74*, 1510–1512.
49. Aernouts, T.; Geens, W.; Poortmans, J.; Heremans, P.; Borghs, S.; Mertens, R. Extraction of bulk and contact components of the series resistance in organic bulk donor-acceptor-heterojunctions. *Thin Solid Films* **2002**, *403–404*, 297–301.
50. Frohne, H.; Müller, D.C.; Meerholz, K. Continuously variable hole injection in organic light emitting diodes. *ChemPhysChem* **2002**, *3*, 707–711.
51. Frohne, H.; Shaheen, S.E.; Brabec, C.J.; Müller, D.C.; Sariciftci, N.S.; Meerholz, K. Influence of the anodic work function on the performance of organic solar cells. *ChemPhysChem* **2002**, *3*, 795–799.
52. Li, G.; Chu, C.-W.; Shrotriya, V.; Huang, J.; Yang, Y. Efficient inverted polymer solar cells. *Appl. Phys. Lett.* **2006**, *88*, doi:10.1063/1.2212270.

53. Kim, Y.; Ballantyne, A.M.; Nelson, J.; Bradley, D.D.C. Effects of thickness and thermal annealing of the PEDOT:PSS layer on the performance of polymer solar cells. *Org. Electron.* **2009**, *10*, 205–209.
54. De Jong, M.P.; van Ijzendoorn, L.J.; de Voigt, M.J.A. Stability of the interface between indium-tin-oxide and poly(3,4-ethylenedioxythiophene)/poly(styrenesulfonate) in polymer light-emitting diodes. *Appl. Phys. Lett.* **2000**, *77*, 2255–2257.
55. Kim, H.; Nam, S.; Lee, H.; Woo, S.; Ha, C.-S.; Ree, M.; Kim, Y. Influence of controlled acidity of hole-collecting buffer layers on the performance and lifetime of polymer:fullerene solar cells. *J. Phys. Chem. C* **2011**, *115*, 13502–13510.
56. Meng, Y.; Hu, Z.; Ai, N.; Jiang, Z.; Wang, J.; Peng, J.; Cao, Y. Improving the stability of bulk heterojunction solar cells by incorporating pH-neutral PEDOT:PSS as the hole transport layer. *ACS Appl. Mater. Interfaces* **2014**, *6*, 5122–5129.
57. Zhang, W.; Zhao, B.; He, Z.; Zhao, X.; Wang, H.; Yang, S.; Wu, H.; Cao, Y. High-efficiency ITO-free polymer solar cells using highly conductive PEDOT:PSS/surfactant bilayer transparent anodes. *Energy Environ. Sci.* **2013**, *6*, 1956–1964.
58. Mengistie, D.A.; Ibrahim, M.A.; Wang, P.-C.; Chu, C.-W. Highly conductive PEDOT:PSS treated with formic acid for ito-free polymer solar cells. *ACS Appl. Mater. Interfaces* **2014**, *6*, 2292–2299.
59. Choi, M.-R.; Han, T.-H.; Lim, K.-G.; Woo, S.-H.; Huh, D.H.; Lee, T.-W. Soluble self-doped conducting polymer compositions with tunable work function as hole injection/extraction layers in organic optoelectronics. *Angew. Chem. Int. Ed.* **2011**, *50*, 6274–6277.
60. Lee, T.W.; Chung, Y.; Kwon, O.; Park, J.J. Self-organized gradient hole injection to improve the performance of polymer electroluminescent devices. *Adv. Funct. Mater.* **2007**, *17*, 390–396.
61. Wu, H.; Huang, F.; Mo, Y.; Yang, W.; Wang, D.; Peng, J.; Cao, Y. Efficient electron injection from a bilayer cathode consisting of aluminum and alcohol-/water-soluble conjugated polymers. *Adv. Mater.* **2004**, *16*, 1826–1830.
62. Duan, C.; Zhang, K.; Zhong, C.; Huang, F.; Cao, Y. Recent advances in water/alcohol-soluble π -conjugated materials: New materials and growing applications in solar cells. *Chem. Soc. Rev.* **2013**, *42*, 9071–9104.
63. He, Z.; Zhong, C.; Huang, X.; Wong, W.-Y.; Wu, H.; Chen, L.; Su, S.; Cao, Y. Simultaneous enhancement of open-circuit voltage, short-circuit current density, and fill factor in polymer solar cells. *Adv. Mater.* **2011**, *23*, 4636–4643.
64. Luo, J.; Wu, H.; He, C.; Li, A.; Yang, W.; Cao, Y. Enhanced open-circuit voltage in polymer solar cells. *Appl. Phys. Lett.* **2009**, *95*, doi:10.1063/1.3157278.
65. Zhao, Y.; Xie, Z.; Qin, C.; Qu, Y.; Geng, Y.; Wang, L. Enhanced charge collection in polymer photovoltaic cells by using an ethanol-soluble conjugated polyfluorene as cathode buffer layer. *Sol. Energy Mater. Sol. Cells* **2009**, *93*, 604–608.
66. Na, S.-I.; Oh, S.-H.; Kim, S.-S.; Kim, D.-Y. Efficient organic solar cells with polyfluorene derivatives as a cathode interfacial layer. *Org. Electron.* **2009**, *10*, 496–500.
67. He, C.; Zhong, C.; Wu, H.; Yang, R.; Yang, W.; Huang, F.; Bazan, G.C.; Cao, Y. Origin of the enhanced open-circuit voltage in polymer solar cells via interfacial modification using conjugated polyelectrolytes. *J. Mater. Chem.* **2010**, *20*, 2617–2622.

68. Seo, J.H.; Gutacker, A.; Sun, Y.; Wu, H.; Huang, F.; Cao, Y.; Scherf, U.; Heeger, A.J.; Bazan, G.C. Improved high-efficiency organic solar cells via incorporation of a conjugated polyelectrolyte interlayer. *J. Am. Chem. Soc.* **2011**, *133*, 8416–8419.
69. Seo, J.H.; Gutacker, A.; Walker, B.; Cho, S.; Garcia, A.; Yang, R.; Nguyen, T.-Q.; Heeger, A.J.; Bazan, G.C. Improved injection in n-type organic transistors with conjugated polyelectrolytes. *J. Am. Chem. Soc.* **2009**, *131*, 18220–18221.
70. Zhou, H.; Zhang, Y.; Seifert, J.; Collins, S.D.; Luo, C.; Bazan, G.C.; Nguyen, T.-Q.; Heeger, A.J. High-efficiency polymer solar cells enhanced by solvent treatment. *Adv. Mater.* **2013**, *25*, 1646–1652.
71. Yang, T.; Wang, M.; Duan, C.; Hu, X.; Huang, L.; Peng, J.; Huang, F.; Gong, X. Inverted polymer solar cells with 8.4% efficiency by conjugated polyelectrolyte. *Energy Environ. Sci.* **2012**, *5*, 8208–8214.
72. Cheng, Y.-J.; Hsieh, C.-H.; He, Y.; Hsu, C.-S.; Li, Y. Combination of indene-C₆₀ bis-adduct and cross-linked fullerene interlayer leading to highly efficient inverted polymer solar cells. *J. Am. Chem. Soc.* **2010**, *132*, 17381–17383.
73. Woo, S.; Kim, H.W.; Kim, H.; Yi, Y.; Lyu, H.-K.; Kim, Y. 8.9% Single-stack inverted polymer solar cells with electron-rich polymer nanolayer-modified inorganic electron-collecting buffer layers. *Adv. Energy Mater.* **2014**, *4*, doi:10.1002/aenm.201301692.
74. Yang, D.; Fu, P.; Zhang, F.; Wang, N.; Zhang, J.; Li, C. High efficiency inverted polymer solar cells with room-temperature titanium oxide/polyethylenimine films as electron transport layers. *J. Mater. Chem. A* **2014**, *2*, 17281–17285.
75. Pho, T.V.; Kim, H.; Seo, J.H.; Heeger, A.J.; Wudl, F. Quinacridone-based electron transport layers for enhanced performance in bulk-heterojunction solar cells. *Adv. Funct. Mater.* **2011**, *21*, 4338–4341.
76. Lu, K.; Yuan, J.; Peng, J.; Huang, X.; Cui, L.; Jiang, Z.; Wang, H.-Q.; Ma, W. New solution-processable small molecules as hole-transporting layer in efficient polymer solar cells. *J. Mater. Chem. A* **2013**, *1*, 14253–14261.
77. Chen, D.; Zhou, H.; Liu, M.; Zhao, W.-M.; Su, S.-J.; Cao, Y. Novel cathode interlayers based on neutral alcohol-soluble small molecules with a triphenylamine core featuring polar phosphonate side chains for high-performance polymer light-emitting and photovoltaic devices. *Macromol. Rapid Commun.* **2013**, *34*, 595–603.
78. Zhang, W.; Wu, Y.; Bao, Q.; Gao, F.; Fang, J. Morphological control for highly efficient inverted polymer solar cells via the backbone design of cathode interlayer materials. *Adv. Energy Mater.* **2014**, *4*, doi:10.1002/aenm.201400359.
79. Tan, W.-Y.; Wang, R.; Li, M.; Liu, G.; Chen, P.; Li, X.-C.; Lu, S.-M.; Zhu, H.L.; Peng, Q.-M.; Zhu, X.-H.; *et al.* Lending triarylphosphine oxide to phenanthroline: A facile approach to high-performance organic small-molecule cathode interfacial material for organic photovoltaics utilizing air-stable cathodes. *Adv. Funct. Mater.* **2014**, *24*, 6540–6547.
80. Zhang, Z.-G.; Qi, B.; Jin, Z.; Chi, D.; Qi, Z.; Li, Y.; Wang, J. Perylene diimides: A thickness-insensitive cathode interlayer for high performance polymer solar cells. *Energy Environ. Sci.* **2014**, *7*, 1966–1973.

81. Cheng, X.; Sun, S.; Chen, Y.; Gao, Y.; Ai, L.; Jia, T.; Li, F.; Wang, Y. A water-soluble metallophthalocyanine derivative as a cathode interlayer for highly efficient polymer solar cells. *J. Mater. Chem. A* **2014**, *2014*, doi:10.1039/C4TA01586J.
82. Wei, Q.; Nishizawa, T.; Tajima, K.; Hashimoto, K. Self-organized buffer layers in organic solar cells. *Adv. Mater.* **2008**, *20*, 2211–2216.
83. Wei, Q.; Tajima, K.; Tong, Y.; Ye, S.; Hashimoto, K. Surface-segregated monolayers: A new type of ordered monolayer for surface modification of organic semiconductors. *J. Am. Chem. Soc.* **2009**, *131*, 17597–17604.
84. Wang, N.; Sun, L.; Zhang, X.; Bao, X.; Zheng, W.; Yang, R. Easily-accessible fullereneol as a cathode buffer layer for inverted organic photovoltaic devices. *RSC Adv.* **2014**, *4*, 25886–25891.
85. Li, X.; Zhang, W.; Wu, Y.; Min, C.; Fang, J. High performance polymer solar cells with a polar fullerene derivative as the cathode buffer layer. *J. Mater. Chem. A* **2013**, *1*, 12413–12416.
86. Zhang, Z.-G.; Li, H.; Qi, B.; Chi, D.; Jin, Z.; Qi, Z.; Hou, J.; Li, Y.; Wang, J. Amine group functionalized fullerene derivatives as cathode buffer layers for high performance polymer solar cells. *J. Mater. Chem. A* **2013**, *1*, 9624–9629.
87. Page, Z.A.; Liu, Y.; Duzhko, V.V.; Russell, T.P.; Emrick, T. Fulleropyrrolidine interlayers: Tailoring electrodes to raise organic solar cell efficiency. *Science* **2014**, *346*, 441–444.
88. Cho, N.; Li, C.-Z.; Yip, H.-L.; Jen, A.K.Y. *In situ* doping and crosslinking of fullerenes to form efficient and robust electron-transporting layers for polymer solar cells. *Energy Environ. Sci.* **2014**, *7*, 638–643.
89. Li, C.-Z.; Chang, C.-Y.; Zang, Y.; Ju, H.-X.; Chueh, C.-C.; Liang, P.-W.; Cho, N.; Ginger, D.S.; Jen, A.K.Y. Suppressed charge recombination in inverted organic photovoltaics via enhanced charge extraction by using a conductive fullerene electron transport layer. *Adv. Mater.* **2014**, *26*, 6262–6267.
90. Liu, J.; Durstock, M.; Dai, L. Graphene oxide derivatives as hole- and electron-extraction layers for high-performance polymer solar cells. *Energy Environ. Sci.* **2014**, *7*, 1297–1306.
91. Li, S.-S.; Tu, K.-H.; Lin, C.-C.; Chen, C.-W.; Chhowalla, M. Solution-processable graphene oxide as an efficient hole transport layer in polymer solar cells. *ACS Nano* **2010**, *4*, 3169–3174.
92. Murray, I.P.; Lou, S.J.; Cote, L.J.; Loser, S.; Kadleck, C.J.; Xu, T.; Szarko, J.M.; Rolczynski, B.S.; Johns, J.E.; Huang, J.; *et al.* Graphene oxide interlayers for robust, high-efficiency organic photovoltaics. *J. Phys. Chem. Lett.* **2011**, *2*, 3006–3012.
93. Smith, C.T.G.; Rhodes, R.W.; Beliatas, M.J.; Jayawardena Imalka, K.D.J.; Rozanski, L.J.; Mills, C.A.; Silva, S.R.P. Graphene oxide hole transport layers for large area, high efficiency organic solar cells. *Appl. Phys. Lett.* **2014**, *105*, doi:10.1063/1.4893787.
94. Stratakis, E.; Savva, K.; Konios, D.; Petridis, C.; Kymakis, E. Improving the efficiency of organic photovoltaics by tuning the work function of graphene oxide hole transporting layers. *Nanoscale* **2014**, *6*, 6925–6931.
95. Yang, D.; Zhou, L.; Yu, W.; Zhang, J.; Li, C. Work-function-tunable chlorinated graphene oxide as an anode interface layer in high-efficiency polymer solar cells. *Adv. Energy Mater.* **2014**, *2014*, doi:10.1002/aenm.201400591.

96. Kim, S.-H.; Lee, C.-H.; Yun, J.-M.; Noh, Y.-J.; Kim, S.-S.; Lee, S.; Jo, S.M.; Joh, H.-I.; Na, S.-I. Fluorine-functionalized and simultaneously reduced graphene oxide as a novel hole transporting layer for highly efficient and stable organic photovoltaic cells. *Nanoscale* **2014**, *6*, 7183–7187.
97. Liu, J.; Xue, Y.; Dai, L. Sulfated graphene oxide as a hole-extraction layer in high-performance polymer solar cells. *J. Phys. Chem. Lett.* **2012**, *3*, 1928–1933.
98. Kakavelakis, G.; Konios, D.; Stratakis, E.; Kymakis, E. Enhancement of the efficiency and stability of organic photovoltaic devices via the addition of a lithium-neutralized graphene oxide electron-transporting layer. *Chem. Mater.* **2014**, *20*, 5988–5993.
99. Jayawardena, K.D.G.I.; Rhodes, R.; Gandhi, K.K.; Prabhath, M.R.R.; Dabera, G.D.M.R.; Beliatas, M.J.; Rozanski, L.J.; Henley, S.J.; Silva, S.R.P. Solution processed reduced graphene oxide/metal oxide hybrid electron transport layers for highly efficient polymer solar cells. *J. Mater. Chem. A* **2013**, *1*, 9922–9927.
100. Small, C.E.; Chen, S.; Subbiah, J.; Amb, C.M.; Tsang, S.-W.; Lai, T.-H.; Reynolds, J.R.; So, F. High-efficiency inverted dithienogermole-thienopyrrolodione-based polymer solar cells. *Nat. Photon.* **2012**, *6*, 115–120.
101. Wang, D.H.; Kim, J.K.; Seo, J.H.; Park, I.; Hong, B.H.; Park, J.H.; Heeger, A.J. Transferable graphene oxide by stamping nanotechnology: Electron-transport layer for efficient bulk-heterojunction solar cells. *Angew. Chem. Int. Ed.* **2013**, *52*, 2874–2880.
102. Arango, A.C.; Johnson, L.R.; Bliznyuk, V.N.; Schlesinger, Z.; Carter, S.A.; Hörhold, H.H. Efficient titanium oxide/conjugated polymer photovoltaics for solar energy conversion. *Adv. Mater.* **2000**, *12*, 1689–1692.
103. van Hal, P.A.; Wienk, M.M.; Kroon, J.M.; Verhees, W.J.H.; Slooff, L.H.; van Gennip, W.J.H.; Jonkheijm, P.; Janssen, R.A.J. Photoinduced electron transfer and photovoltaic response of a MDMO–PPV:TiO₂ bulk-heterojunction. *Adv. Mater.* **2003**, *15*, 118–121.
104. Yeon Song, M.; Kim, K.-J.; Kim, D.Y. Enhancement of photovoltaic characteristics using a PEDOT interlayer in TiO₂/MEHPPV heterojunction devices. *Sol. Energy Mater. Sol. Cells* **2005**, *85*, 31–39.
105. Watanabe, A.; Kasuya, A. Effect of atmospheres on the open-circuit photovoltage of nanoporous TiO₂/poly(3-hexylthiophene) heterojunction solar cell. *Thin Solid Films* **2005**, *483*, 358–366.
106. Kim, J.Y.; Kim, S.H.; Lee, H.H.; Lee, K.; Ma, W.; Gong, X.; Heeger, A.J. New architecture for high-efficiency polymer photovoltaic cells using solution-based titanium oxide as an optical spacer. *Adv. Mater.* **2006**, *18*, 572–576.
107. Park, M.-H.; Li, J.-H.; Kumar, A.; Li, G.; Yang, Y. Doping of the metal oxide nanostructure and its influence in organic electronics. *Adv. Funct. Mater.* **2009**, *19*, 1241–1246.
108. Roest, A.L.; Kelly, J.J.; Vanmaekelbergh, D.; Meulenkaamp, E.A. Staircase in the electron mobility of a ZnO quantum dot assembly due to shell filling. *Phys. Rev. Lett.* **2002**, *89*, 036801.
109. Shirakawa, T.; Umeda, T.; Hashimoto, Y.; Fujii, A.; Yoshino, K. Effect of ZnO layer on characteristics of conducting polymer/C₆₀ photovoltaic cell. *J. Phys. D Appl. Phys.* **2004**, *37*, doi:10.1088/0022-3727/37/6/007.
110. White, M.S.; Olson, D.C.; Shaheen, S.E.; Kopidakis, N.; Ginley, D.S. Inverted bulk-heterojunction organic photovoltaic device using a solution-derived ZnO underlayer. *Appl. Phys. Lett.* **2006**, *89*, doi:10.1063/1.2359579

111. Amb, C.M.; Chen, S.; Graham, K.R.; Subbiah, J.; Small, C.E.; So, F.; Reynolds, J.R. Dithienogermole as a fused electron donor in bulk heterojunction solar cells. *J. Am. Chem. Soc.* **2011**, *133*, 10062–10065.
112. Chen, S.; Small, C.E.; Amb, C.M.; Subbiah, J.; Lai, T.-H.; Tsang, S.-W.; Manders, J.R.; Reynolds, J.R.; So, F. Inverted polymer solar cells with reduced interface recombination. *Adv. Energy Mater.* **2012**, *2*, 1333–1337.
113. Sun, Y.; Seo, J.H.; Takacs, C.J.; Seifert, J.; Heeger, A.J. Inverted polymer solar cells integrated with a low-temperature-annealed sol-gel-derived ZnO film as an electron transport layer. *Adv. Mater.* **2011**, *23*, 1679–1683.
114. Hsieh, C.-H.; Cheng, Y.-J.; Li, P.-J.; Chen, C.-H.; Dubosc, M.; Liang, R.-M.; Hsu, C.-S. Highly efficient and stable inverted polymer solar cells integrated with a cross-linked fullerene material as an interlayer. *J. Am. Chem. Soc.* **2010**, *132*, 4887–4893.
115. Mrowec, S.; Grzesik, Z. Oxidation of nickel and transport properties of nickel oxide. *J. Phys. Chem. Solids* **2004**, *65*, 1651–1657.
116. Irwin, M.D.; Buchholz, D.B.; Hains, A.W.; Chang, R.P.H.; Marks, T.J. P-type semiconducting nickel oxide as an efficiency-enhancing anode interfacial layer in polymer bulk-heterojunction solar cells. *Proc. Natl. Acad. Sci. USA* **2008**, *105*, 2783–2787.
117. Irwin, M.D.; Servaites, J.D.; Buchholz, D.B.; Leever, B.J.; Liu, J.; Emery, J.D.; Zhang, M.; Song, J.-H.; Durstock, M.F.; Freeman, A.J., *et al.* Structural and electrical functionality of NiO interfacial films in bulk heterojunction organic solar cells. *Chem. Mater.* **2011**, *23*, 2218–2226.
118. Ratcliff, E.L.; Meyer, J.; Steirer, K.X.; Garcia, A.; Berry, J.J.; Ginley, D.S.; Olson, D.C.; Kahn, A.; Armstrong, N.R. Evidence for near-surface NiOOH species in solution-processed NiOx selective interlayer materials: Impact on energetics and the performance of polymer bulk heterojunction photovoltaics. *Chem. Mater.* **2011**, *23*, 4988–5000.
119. Steirer, K.X.; Ndione, P.F.; Widjonarko, N.E.; Lloyd, M.T.; Meyer, J.; Ratcliff, E.L.; Kahn, A.; Armstrong, N.R.; Curtis, C.J.; Ginley, D.S.; *et al.* Enhanced efficiency in plastic solar cells via energy matched solution processed NiOx interlayers. *Adv. Energy Mater.* **2011**, *1*, 813–820.
120. Manders, J.R.; Tsang, S.-W.; Hartel, M.J.; Lai, T.-H.; Chen, S.; Amb, C.M.; Reynolds, J.R.; So, F. Solution-processed nickel oxide hole transport layers in high efficiency polymer photovoltaic cells. *Adv. Funct. Mater.* **2013**, *23*, 2993–3001.
121. Song, C.K.; White, A.C.; Zeng, L.; Leever, B.J.; Clark, M.D.; Emery, J.D.; Lou, S.J.; Timalina, A.; Chen, L.X.; Bedzyk, M.J.; *et al.* Systematic investigation of organic photovoltaic cell charge injection/performance modulation by dipolar organosilane interfacial layers. *ACS Appl. Mater. Interfaces* **2013**, *5*, 9224–9240.
122. Song, C.K.; Luck, K.A.; Zhou, N.; Zeng, L.; Heitzer, H.M.; Manley, E.F.; Goldman, S.; Chen, L.X.; Ratner, M.A.; Bedzyk, M.J.; *et al.* “Supersaturated” self-assembled charge-selective interfacial layers for organic solar cells. *J. Am. Chem. Soc.* **2014**, *136*, 17762–17773.
123. Motiei, L.; Yao, Y.; Choudhury, J.; Yan, H.; Marks, T.J.; Boom, M.E.V.D.; Facchetti, A. Self-propagating molecular assemblies as interlayers for efficient inverted bulk-heterojunction solar cells. *J. Am. Chem. Soc.* **2010**, *132*, 12528–12530.

124. Song, Y.; Yan, L.; Zhou, Y.; Song, B.; Li, Y. Lowering the work function of ito by covalent surface grafting of aziridine: Application in inverted polymer solar cells. *Adv. Mater. Interfaces* **2015**, *2*, doi:10.1002/admi.201400397.
125. Hains, A.W.; Liu, J.; Martinson, A.B.F.; Irwin, M.D.; Marks, T.J. Anode interfacial tuning via electron-blocking/hole-transport layers and indium tin oxide surface treatment in bulk-heterojunction organic photovoltaic cells. *Adv. Funct. Mater.* **2010**, *20*, 595–606.
126. Cho, N.; Yip, H.-L.; Davies, J.A.; Kazarinoff, P.D.; Zeigler, D.F.; Durban, M.M.; Segawa, Y.; O'Malley, K.M.; Luscombe, C.K.; Jen, A.K.Y. *In-situ* crosslinking and n-doping of semiconducting polymers and their application as efficient electron-transporting materials in inverted polymer solar cells. *Adv. Energy Mater.* **2011**, *1*, 1148–1153.
127. Moon, B.J.; Cho, S.; Lee, K.S.; Bae, S.; Lee, S.; Hwang, J.Y.; Angadi, B.; Yi, Y.; Park, M.; Son, D.I. Enhanced photovoltaic performance of inverted polymer solar cells utilizing multifunctional quantum-dot monolayers. *Adv. Energy Mater.* **2014**, *5*, doi:10.1002/aenm.201401130.
128. Yaacobi-Gross, N.; Treat, N.D.; Pattanasattayavong, P.; Faber, H.; Perumal, A.K.; Stingelin, N.; Bradley, D.D.C.; Stavrinou, P.N.; Heeney, M.; Anthopoulos, T.D. High-efficiency organic photovoltaic cells based on the solution-processable hole transporting interlayer copper thiocyanate (CuSCN) as a replacement for PEDOT:PSS. *Adv. Energy Mater.* **2014**, *5*, doi:10.1002/aenm.201401529.

© 2015 by the authors; licensee MDPI, Basel, Switzerland. This article is an open access article distributed under the terms and conditions of the Creative Commons Attribution license (<http://creativecommons.org/licenses/by/4.0/>).